Rock Mechanics and Rock Engineering (2019) 52:5137–5160
https://doi.org/10.1007/s00603-019-01851-3

ORIGINAL PAPER

Investigating Hydraulic Fracturing Complexity in Naturally Fractured Rock Masses Using Fully Coupled Multiscale Numerical Modeling

Fengshou Zhang[1,2] · **Branko Damjanac**[3] · **Shawn Maxwell**[4]

Received: 9 November 2018 / Accepted: 15 May 2019 / Published online: 24 May 2019

Abstract
Naturally fractured rock mass is highly inhomogeneous and contains geological discontinuities at various length scales. Hydraulic fracture stimulation in such a medium could result in complex fracture systems instead of simple planar fractures. In this study, we carried out fully coupled multiscale numerical analysis to investigate some key coupled processes of fluid-driven fracture propagation in naturally fractured rock mass. The numerical analysis follows the concept of the synthetic rock mass (SRM) method initially developed in the discrete element method (DEM). We introduce a total of five case study examples, including fracture initiation and near wellbore tortuosity, hydraulic fracture interaction with natural fractures, multi-stage hydraulic fracturing with discrete fracture network (DFN), in-fill well fracturing and frac hits after depletion-induced stress change, and induced seismicity associated with fault reactivation. Through those case studies, we demonstrate that with an advanced numerical modeling tool, the complex fracturing associated with hydraulic fracturing in naturally fractured rock mass can be qualitatively analyzed and the extent of various uncertainties can be assessed.

Keywords Hydraulic fracturing · Naturally fractured rock mass · Fracturing complexity · Near wellbore tortuosity · Frac hits · Induced seismicity

1 Introduction

1.1 Problem Definition

Hydraulic fracturing refers to the process of fluid-driven fracture propagation in solids. The most common engineering application of hydraulic fracturing is the stimulation of oil and gas reservoirs by injecting high-pressure fluid containing proppant particles into the rock formations to form high-permeability paths for hydrocarbon (Economides and Nolte 2000). The basic mechanics of hydraulic fracturing have been extensively studied in the past few decades (Khristianovic and Zheltov 1955; Howard and Fast 1957; Hubbert and Willis 1957; Perkins and Kern 1961; Barenblatt 1962; Nordgren 1972; Geertsma and Haafkens 1979). The problem of hydraulic fracture propagation involves processes taking place on different time and length scales, created by the interplay of a few competing physical processes, including viscous fluid flow in the fracture, fracture propagation at the tip, fluid front lag behind the fracture tip, fluid leak-off into the reservoir, and elastic deformation of the rock matrix (Detournay 2016). The interaction of these individual processes results in complexities in fracture growth, especially in heterogeneous lithology.

Horizontal drilling and multi-stage hydraulic fracturing have been the two key factors allowing for the successful exploitation of tight gas, shale gas, and other unconventional resources since the middle of the 2000s. Multi-stage fracturing technique makes the effective stimulation of low-permeability reservoirs possible and, thus, has facilitated the development of unconventional hydrocarbon resources. The number of hydraulic fracturing jobs along horizontal wells has been greatly increasing, leading to the "shale gas revolution" that started in North America and is currently spreading globally (King 2010).

✉ Fengshou Zhang
fengshou.zhang@tongji.edu.cn

[1] Key Laboratory of Geotechnical and Underground Engineering of Ministry of Education, Tongji University, Shanghai 200092, China

[2] Department of Geotechnical Engineering, College of Civil Engineering, Tongji University, Shanghai 200092, China

[3] Itasca Consulting Group, Inc., Minneapolis, MN 55401, USA

[4] MaxSeis LLC., Calgary, AB T2P 3N9, Canada

Following the boom of hydraulic fracturing, there is an urgent need for the development of hydraulic fracturing theories suitable for application to unconventional resource recovery. Traditional hydraulic fracturing solutions and models are based on the assumptions of simple and planar geometries (Adachi et al. 2007). However, hydraulic fracture networks from multi-stage stimulation of horizontal wells are understood to include complex fracture networks (Maxwell and Cipolla 2011; Warpinski et al. 2013), hence, these basic traditional models are too simplified to be applied to complex geometries in naturally fractured reservoirs. Driven by the increasing research interests in this area, there have been significant improvements in the understanding of critical physical processes and advances in numerical methods used in the field of unconventional hydraulic fracturing. However, commenting on the current status of understanding hydraulic fracturing, Bažant et al. (2014) state that:

> "Although spectacular advances in hydraulic fracturing, also known as fracking, have taken place and many aspects are well understood by now, the topology, geometry, and evolution of the crack system remains an enigma and mechanicians wonder: Why fracking works?"

The statement above reflects the reality that despite the astounding progress that has been made in understanding the mechanics of hydraulic fracturing in naturally fractured rock mass, some fundamental mechanisms are yet to be understood. The precise prediction of fracture geometries remains a great challenge. The current hydraulic fracturing operations for unconventional resource recovery still heavily rely on "trial-and-error" strategies which indicates that a gap between research and practice needs to be bridged.

1.2 Causes of Fracturing Complexity

Even in a homogeneous medium and in the simplest form, hydraulic fracturing is a non-linear and multiscale process, involving strong hydro-mechanical coupling. There are multiple length and time scales, which determine the fracture evolution both temporally and spatially (Detournay 2004, 2016). Geological complexity, uncertainty, and spatial variability of the naturally fractured reservoirs make hydraulic fracturing even more complex. Fairhurst (2013) comments on the characteristic of rock materials as:

> "Rock in situ is arguably the most complex material encountered in any engineering discipline. Deformed and fractured over many millions of years and different tectonic stress regimes, it contains fractures on a wide variety of length scales from microscopic to tectonic plate boundaries."

Thus, the propagation of a hydraulic fracture in naturally fractured rock mass can be expected to interact with geological discontinuities at different length scales. Those geological discontinuities include microcracks, joints, bedding planes, and faults (Fig. 1) and their sizes span from millimeters to kilometers. Meanwhile, the temporal character of a hydraulic fracture could also span a few orders of magnitude, from milliseconds (e.g., fracture initiation), to seconds (e.g., near wellbore propagation), minutes (e.g., height growth), hours (e.g., duration of a frack job), days (e.g., stage interaction), weeks (e.g., well interaction), and extends to years (e.g., fracture closing during production). Those multiscale characteristics of hydraulic fracturing can all contribute to the fracturing complexity.

Another reason contributing to the difficulty of predicting hydraulic fracturing is the uncertainty in the characterization of some crucial controlling reservoir properties, caused by the limited access to relatively deep naturally fractured reservoirs. Due to the complex nature of in situ rock mass fracturing, the characterization of discrete fracture network (DFN) can only be accomplished statistically (Davy et al. 2010). In many instances, data are insufficient for proper statistical characterization of reservoir DFNs. The measurement of in situ stress typically depends on very few well logs. However, strong heterogeneity of horizontal stress is not just found along the vertical direction (Wileveau et al. 2007). There is evidence that the minimum horizontal stress could vary significantly from stage to stage for the same horizontal well (Ma and Zoback 2017). Limited information on in situ conditions of targeted reservoir formations gives rise to large uncertainty of model predictions using any modeling approach.

1.3 Recent Development of Numerical Modeling Techniques

Numerical modeling has been a vital tool to study hydraulic fracturing. Most of the early models were based on the linear

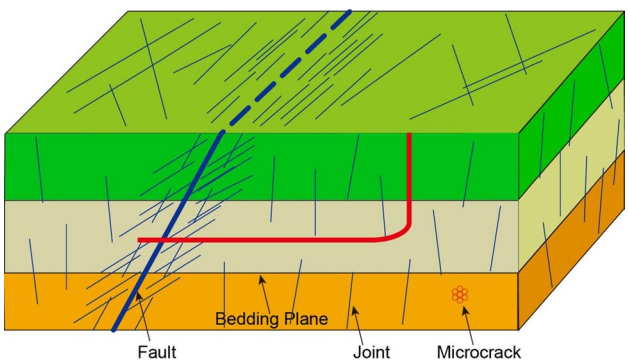

Fig. 1 Schematic of multiscale geological discontinuities in rock mass

elastic fracture mechanics with simple planar geometry (Clifton and Abou-Sayed 1981; Advani et al. 1987, 1990; Carter et al. 2000; Siebrits and Peirce 2002; Adachi et al. 2007). Nevertheless, these models have greatly enhanced the understanding of hydraulic fracturing and helped promote the application of hydraulic fracturing in the oil and gas industry. In recent years, great efforts have been made to develop complex fracture models more suitable for hydraulic fracturing in unconventional reservoirs. Instead of assuming a single planar fracture, the following important processes are typically accounted for in those complex fracturing models:

- hydraulic fracture interaction with geological discontinuities;
- complex hydraulic fracturing with the existence of DFN;
- interference of multiple propagating hydraulic fractures;
- three-dimensional non-planar fracturing propagation; and
- near wellbore fracture initiation and propagation.

Those models can be categorized based on the underlying numerical methods: finite element method (FEM) including cohesive zone method (Chen et al. 2009; Carrier and Granet 2012; Haddad and Seperhrnoori 2015; Deng et al. 2016) and XFEM (Lecampion 2009; Gordeliy and Peirce 2013; Haddad and Sepehrnoori 2016); discrete element method (Zhang et al. 2013a, 2017; Wang et al. 2014; Zhu et al. 2019); lattice method (Damjanac et al. 2016); distinct-element method (Damjanac and Cundall 2016; Zhou et al. 2016; Zhang and Mack 2017; Dontsov and Zhang 2018; Zhang and Dontsov 2018); boundary element method (Zhang et al. 2007; Kresse et al. 2013; Wu and Olson 2015; Tang and Wu 2018); and hybrid method-combined finite-discrete element method, i.e., FDEM (Profit et al. 2016; Lisjak et al. 2017). There are also a few new numerical methods being applied to hydraulic fracturing, such as the material point method (Aimene and Ouenes 2015), peridynamics (Ouchi et al. 2015), and the phase field method (Mikelić et al. 2015; Miehe and Mauthe 2016).

A comprehensive review of all methods used for simulation of hydraulic fracturing is out of the scope of this paper. Only a few representative references are chosen for each category. A more complete list of references can be found in the recent review papers about unconventional hydraulic fracturing modeling (Li et al. 2015; Weng 2015; Dahi Taleghani et al. 2016; Lecampion et al. 2018).

1.4 Paper Objectives and Organization

In this paper, the results of numerical analyses of a series of multiscale hydraulic fracturing problems in naturally fractured rock mass are presented. The goal is to demonstrate some recent attempts to address a few key coupled processes during hydraulic fracturing by employing various numerical tools. By choosing suitable numerical schemes and properly constructing the fracturing models, aspects of the fracturing complexity can be understood and some insights for improving the engineering design can be provided.

The organization of the paper structure is as follows: first, we introduce the numerical schemes and present a few key concepts. Then, a total of five case studies focusing on different aspects of hydraulic fracturing are presented. The first case study is about the modeling of fracture initiation and near wellbore complexity, with the explicit representation of perforation tunnels and borehole. The second case study discusses the mechanism of hydraulic fracture interaction with natural fractures, with the combination of both two- and three-dimensional analysis. The third case study is about multi-stage hydraulic fracturing, including the generation of discrete fracture network and the integration of microseismic interpretation. In the fourth case study, we address the challenges in the process of in-fill well fracturing under the condition of depletion-induced stress change. In the fifth case study, we discuss the mechanism of injection-induced seismicity, with a specific emphasis on the hydraulic-fracturing-induced fault reactivation.

2 Numerical Solutions

The numerical schemes used in the case studies of this paper include the distinct-element method, particle flow codes, the lattice algorithm, and the finite difference method. For the sake of brevity, the detailed descriptions of those numerical schemes are not presented in this paper. The numerical analysis follows the concept of the synthetic rock mass (SRM) method initially developed in the discrete element method (DEM). The SRM model has been developed recently as a more realistic representation of rock mass containing geological discontinuities (Mas Ivars et al. 2011). The SRM for hydraulic fracturing consists of four essential parts (Damjanac and Cundall 2016; Damjanac et al. 2016): (1) the intact rock representation by the boned particle model (BPM) (Potyondy and Cundall 2004); (2) the 3D fracture network representation, or DFN; (3) the smooth joint model (SJM) used to implement the fractures (joints) in the BPM; and (4) the fluid flow network of pipes and reservoirs for the fluid transport in both rock matrix and natural/hydraulic fractures. These four components are integrated to provide fully coupled hydro-mechanical analysis of the fluid-driven fracture propagation in a naturally fractured rock mass.

There are a few advantages of applying the SRM model for simulating hydraulic fracturing in fractured rock mass. First, as inherited from the BPM, SRM exhibits emergent mechanical behaviors that arise from grain (particle) packing and a set of grain and cement properties on

the microscale. Phenomenological damage laws are not required. Instead, the fluid-driven fracture propagation evolves naturally because of tensile or shear breakages of bonding. Second, material inhomogeneity can be naturally applied by adjusting the properties of grains and cement. Third, there is no need to predefine trajectories of hydraulic fractures. Non-planar fracture trajectories, intersections or branching are part of the model solution and can be explicitly modeled. Fourth, synthetic microseismicity can be generated as a result of fracture sliding calculated in the models.

Integration of SRM modeling for hydraulic fracturing in a naturally fractured rock mass with microseismic analysis in the field could provide a feedback loop in which SRM can be enhanced and constrained (Maxwell et al. 2015b). The SRM models can output the synthetic microseismicity and injection pressure. The model can then be calibrated by comparing those with the field data. The calibrated model can be used for better interpretation of the field data and can serve as an engineering tool for the forward analysis.

As pointed out by Starfield and Cundall (1988), most of the rock mechanics models fall into the class of "data limited" and "poorly understood" problems and one typically does not have enough information to model it unambiguously (Fig. 2). Because of the multiscale nature and strongly coupled multiphysics, hydraulic fracturing modeling is often considered to be one of the most challenging among all rock mechanics models. For such a complex problem, the modeling philosophy should be as described by Starfield and Cundall (1988):

> "After all, we build models because the real world is too complex for our understanding; it does not help if we build models that are also too complex. The art of modelling lies in determining what aspects of the geology are essential for the model. The challenge is to turn that art into a methodology."

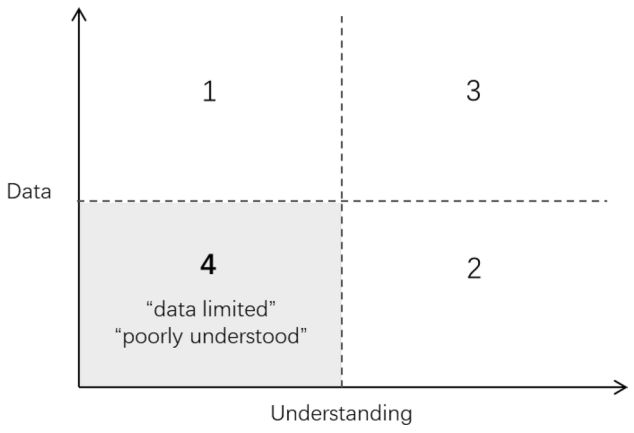

Fig. 2 Classification of numerical modeling problems (after Starfield and Cundall 1988); modeling of hydraulic fracturing belongs to the fourth category

Given the level of complexity, one should not expect a universal model for all hydraulic fracturing problems. Simplification to the studied problem is inevitable but keeping the "essential aspects" of geology in the model is the key. In the past decade, numerous new numerical schemes have been developed. Nevertheless, one should notice that all models have assumptions and limitations. For a given engineering problem, the critical steps for the successful modeling are understanding the basic underlying physics, selection of the suitable modeling scheme, and making some reasonable assumptions. In the next few sections, we present five different case studies with regard to hydraulic fracturing in a naturally fractured rock mass, covering a large range of temporal and spatial scales. For each case study, we state used assumptions and provide justification for the modeling scheme used to address the problem, including the possible limitations in the analysis.

3 Fracture Initiation and Near Wellbore Tortuosity

Understanding the mechanism of fracture initiation and near wellbore tortuosity is of great importance to the optimization of fracturing design and the interpretation of bottomhole pressure (BHP) during hydraulic fracturing treatments. However, numerical modeling of fracture initiation and near wellbore tortuosity have been a great challenge due to the following reasons: first, significantly different characteristic dimensions of borehole and perforation tunnels present a challenge of modeling vastly different length scales in the same model; second, the fracture propagation is complex, including mixed modes of propagation in 3D that result in non-planar geometry; and lastly, the stress redistribution due to the construction of perforation tunnels and borehole, as well as the stress shadow effect caused by the propagation of multiple fractures (Nagel et al. 2013), both dynamically evolving, need to be properly accounted for.

We applied a 3D lattice algorithm to investigate the fracture propagation with explicit modeling of perforation tunnels and borehole (Zhang and Mack 2016). The model is fully coupled hydro-mechanically and can represent detailed geometries at a wide range of scales. A cubical model with 1.22 m edge length was constructed, as shown in Fig. 3. A horizontal borehole is set up with six perforation tunnels along the one-foot borehole segment. The six perforation tunnels form a spiral-shape array with the phasing angle of 60° around the borehole, similar to a typical field perforation pattern. The radius of the borehole is 5.72 cm, with

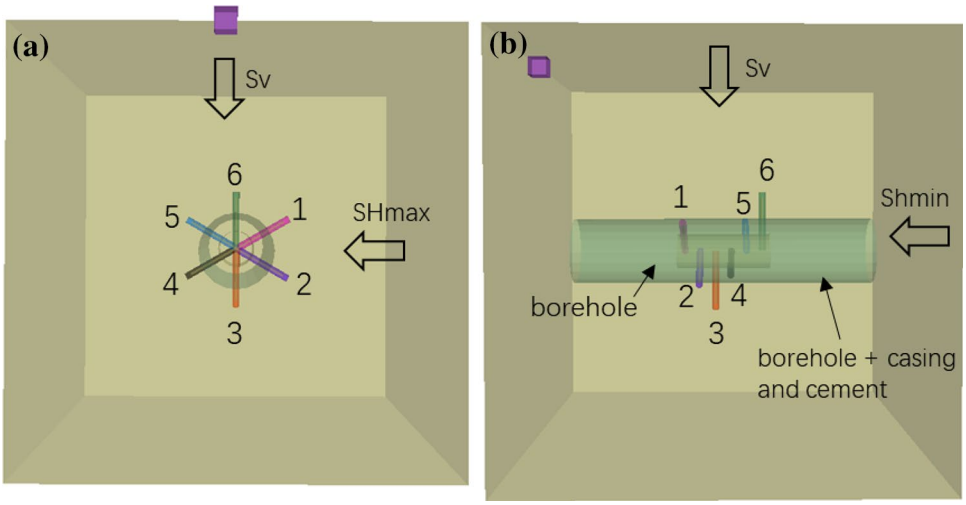

Fig. 3 3D lattice model of hydraulic fracture initiation through perforation tunnels along a horizontal well: **a** lateral view along the Shmin direction, **b** lateral view along the SHmax direction

Table 1 Input parameters in the fracture initiation model with perforations

Rock property	
Elastic modulus (GPa)	33.8
Poisson's ratio	0.208
Toughness (MPa·m$^{0.5}$)	1.35
Stress and pore pressure	
Shmin (MPa)	64.8
SHmax (MPa)	80.0
Sv (MPa)	92.4
PP (MPa)	34.5
Injection parameters	
Injection rate (m^3/s)	0.00265
Fluid viscosity (cp)	1

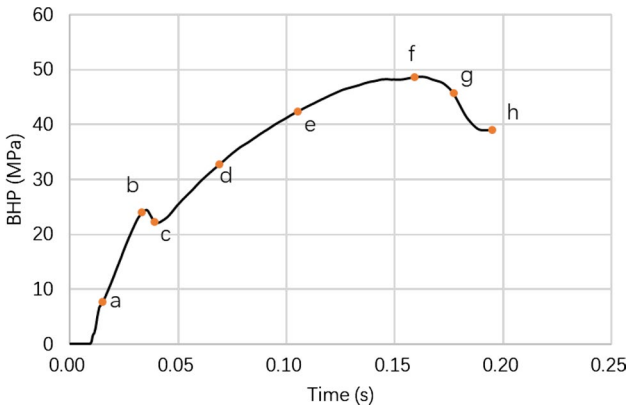

Fig. 4 The BHP versus time; eight intermediate states are chosen to present the results

additional casing wall thickness of 0.856 cm and cement thickness of 4.06 cm. The length of the perforation tunnel (starting from the internal wall of casing) is 17.6 cm and the radius is 0.457 cm. A normal faulting regime is applied to the model. The input parameters for this model are summarized in Table 1.

The modeling is carried out with the following procedure: (1) rock properties and stress are assigned to the cubic block without the borehole and the model is run to reach the initial mechanical equilibrium; (2) the borehole is constructed and the liner and casing are applied before the model is forced to reach the new mechanical equilibrium state again; (3) six perforation tunnels are constructed and the model is equilibrated one more time before injection; and (4) injection is simulated for a specific fluid type and injection rate.

Figure 4 plots the BHP versus time. A total of eight intermediate states, with labels from a to h, are chosen to present the results. The pressure continues climbing when the injection starts, with only a slight pressure drop from state b to state c, until reaching the peak at state f and then declining.

Figures 5 and 6 show configurations of fracture initiation and growth (marked in Fig. 4) from the horizontal borehole in two lateral views, in the Shmin and SHmax directions, respectively. One fracture initiates from the intersection area of each perforation tunnel, those fractures are observed as radial pattern along the Shmin view direction (Fig. 5). Starting from state e, fractures from the first three perforation tunnels begin to coalesce and eventually form a transverse radial hydraulic fracture, while the propagation of the other three fractures from perforations #4, #5, and #6 stops. For the perforation configuration shown in Fig. 3, the two outer perforations, #1 and #6, are expected to be less constrained in terms of stress shadow effect compared to the other four perforations. Therefore, transverse fractures are expected to propagate preferentially from these two positions. Nevertheless, as shown in Fig. 3a, the positions of perforations #1 and #6 relative to the borehole and the neighbor perforations are different (60° difference of phase angle between them). Thus, the propagation conditions for these two fractures are

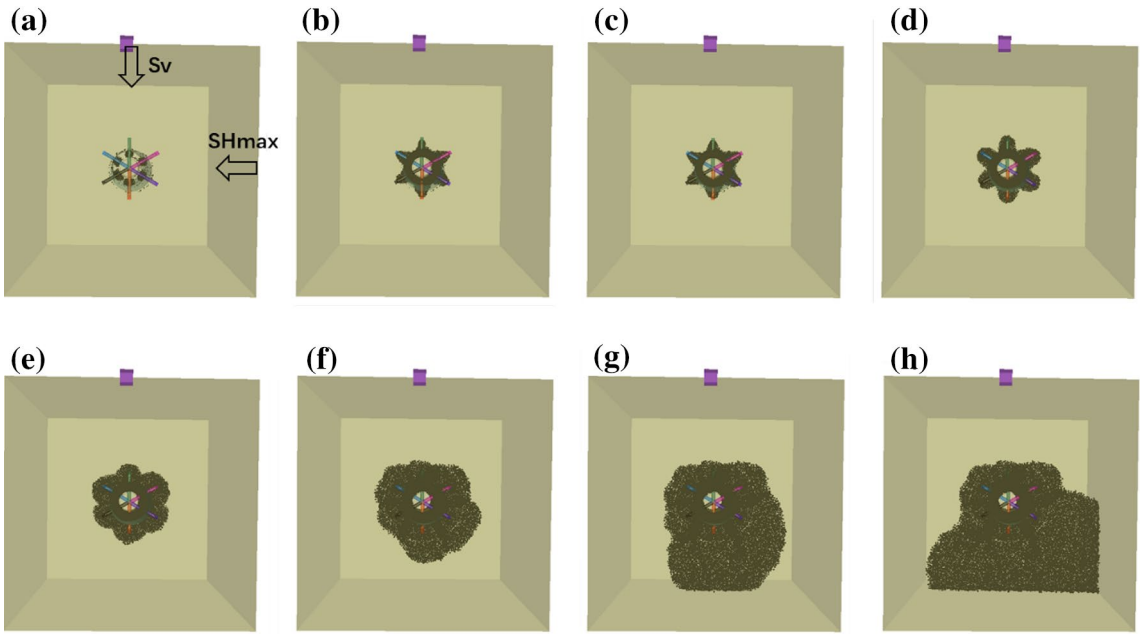

Fig. 5 Shmin direction lateral view of fracture initiation and growth from the horizontal borehole

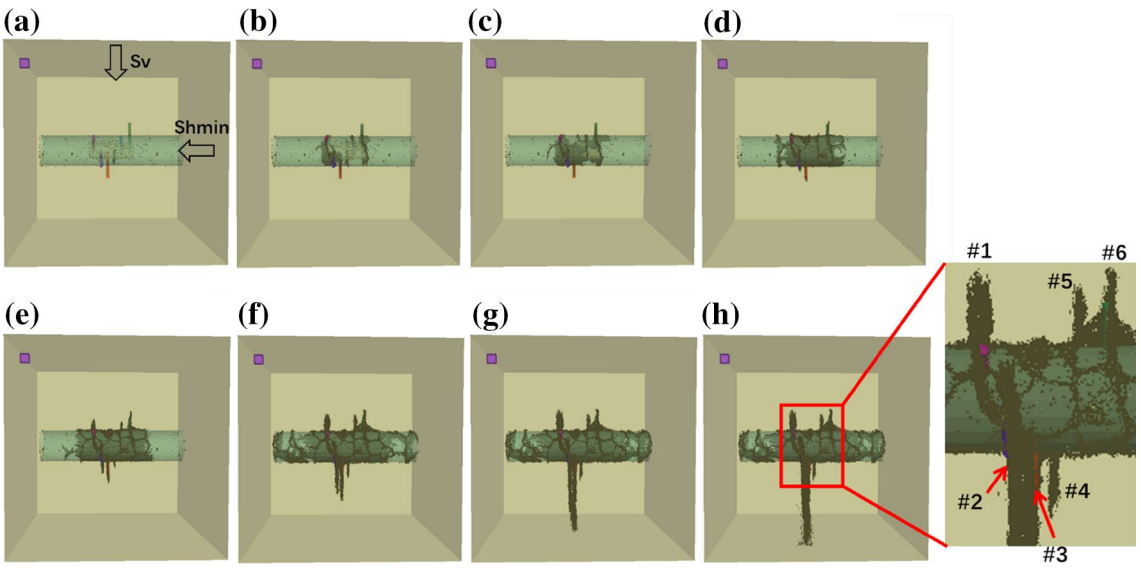

Fig. 6 SHmax direction lateral view of fracture initiation and growth from the horizontal borehole; the magnified figure of stage h indicates that the coalescence of fractures from perforations #2 and #3 forms a single radial hydraulic fracture

not equal. Figures 5 and 6 show that the model favors the propagation of fracture from perforation #1, leading to coalescence with fractures from the nearby perforations #2 and #3 to ultimately form a single radial hydraulic fracture.

The above results show that the fracture initiation and near wellbore tortuosity are complex multiscale problems. The fracture propagation is subjected to the combination of a few key factors (Hou et al. 2018; Zhang et al. 2018). 3D non-planar mixed modes of fracture propagation with the explicit modeling of the stress redistribution around the perforation tunnels and borehole are essential to address this problem. The advanced 3D lattice algorithm in this study helps better understanding of the fracturing profile under different stress conditions and wellbore configurations.

4 Hydraulic Fracture Interaction with Natural Fractures

Hydraulic fracturing in a naturally fractured rock mass is different from conventional hydraulic fracturing because the pre-existing discontinuities in rock mass can greatly impact the propagation of hydraulic fracture. Mineback experiments in the field showed that geological discontinuities significantly affect the overall geometry of hydraulic fracture (Warpinski and Teufel 1987; Jeffrey et al. 2009). Field microseismic observations also indicated that "fracture complexity" may result from interactions between the created hydraulic fracture and pre-existing natural fractures (Maxwell and Cipolla 2011; Maxwell 2014). Thus, the assumption of simple planar fracture geometry is not generally applicable in fractured reservoirs. The hydraulic fracture/natural fracture interaction is an important mechanism during hydraulic fracturing in naturally fractured rock mass.

We developed a two-dimensional hybrid DEM-continuum numerical scheme to study the behavior of a hydraulic fracture crossing natural fractures (Zhang et al. 2017). The fully coupled hybrid scheme utilizes a discrete element model (PFC) for an inner domain, within which the hydraulic fracture propagates and interacts with natural fractures. The inner domain is surrounded by an outer continuum domain (FLAC) (Fig. 7). The hydraulic fracture initiates from the middle of the left boundary (red dot in Fig. 7a), propagates horizontally along the predefined fracture path in the FLAC domain, and then enters the PFC domain. The hybrid DEM-continuum scheme takes the advantages of both DEM and continuum approach for modeling of the multiscale problems like hydraulic fracturing. The DEM domain is used to simulate the particle-scale behavior of rock including the effects of multiple discontinuities while the continuum domain is implemented to allow representation of extended length of the hydraulic fracture in the numerical model and to better approximate the far-field boundary effects. The input parameters in the DEM-continuum model can be found in Table 2.

Three types of basic hydraulic fracture crossing scenario can be identified by varying the stress ratios SHmax/Shmin and the friction coefficient of the natural fracture, as shown in Fig. 8. The first scenario is "no crossing" (Fig. 8a). The hydraulic fracture is arrested after intersecting the natural fracture and a T-shape intersection forms. The natural fracture slips as a result of the interaction with the hydraulic fracture. The second scenario is "offset crossing" (Fig. 8b). The hydraulic fracture forms a T-shape intersection initially, but eventually crosses the natural fracture with an offset. The third scenario is "direct crossing" (Fig. 8c). The hydraulic

Table 2 Input parameters in the DEM-continuum model for hydraulic fracture interaction with natural fractures

Rock property	
Elastic modulus (GPa)	19.4
Poisson's ratio	0.24
Direct tensile strength (MPa)	5.3
Uniaxial compression strength (MPa)	19.0
Toughness (MPa·m$^{0.5}$)	1.20
Natural fracture property	
Normal stiffness (GPa/m)	10.0
Shear stiffness (GPa/m)	10.0
Joint tensile strength (MPa)	0
Cohesion (MPa)	0
Coefficient of friction	0.2, 0.4, 0.5, 0.6, 0.8
Stress and pore pressure	
Shmin (MPa)	20.0
SHmax (MPa)	20.0, 22.0, 26.0, 30.0
PP (MPa)	10.0
Injection parameters	
Injection rate (m^2/s)	0.0015
Fluid viscosity (cp)	10

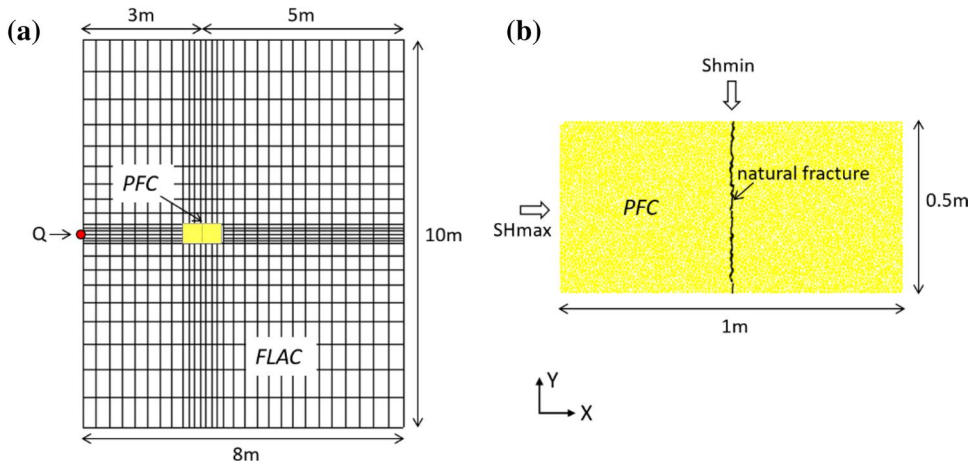

Fig. 7 **a** Simulation domain for the DEM-continuum hybrid model. The yellow rectangle represents the PFC assembly while the black solid lines represent the FLAC mesh; **b** PFC assembly with a natural fracture perpendicular to the SHmax (color figure online)

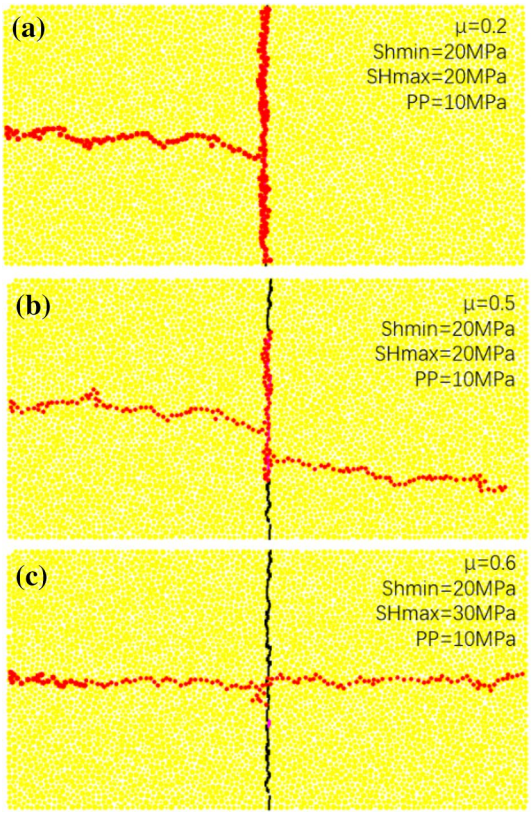

Fig. 8 Three types of interaction between a hydraulic fracture and an orthogonal natural fracture for various stress ratios SHmax/Shmin and the friction coefficient of the natural fracture: **a** no crossing, i.e., T-shape intersection; **b** offset crossing, i.e., crossing with an offset; and **c** direct crossing. The red dots represent the pressure increase at each pore domain along the fracture; the black line represents the natural fracture (color figure online)

fracture crosses the natural fracture without any diversion into the natural fracture.

The net pressure history versus the hydraulic fracture tip location corresponding to the three different crossing scenarios is shown in Fig. 9. For each crossing scenario, the pressure behaves differently after the hydraulic fracture meets the natural fracture and distinct pressure patterns can be identified. For the no-crossing case, the net pressure keeps building up after the hydraulic fracture is arrested by the natural fracture. For the offset crossing case, the net pressure increases first and declines once the hydraulic fracture eventually crosses the natural fracture with an offset. For the direct crossing case, the natural fracture has a minimal effect on the net pressure and is almost the same (about 1.5 MPa) before and after the crossing. The distinct pressure signals shown in Fig. 9, although from two-dimensional analysis, may suggest guidelines for interpreting injection pressure data in the field. A sharp increase of net pressure could indicate that the hydraulic fracture is arrested by a natural fracture or an interface, while a sudden drop of net pressure

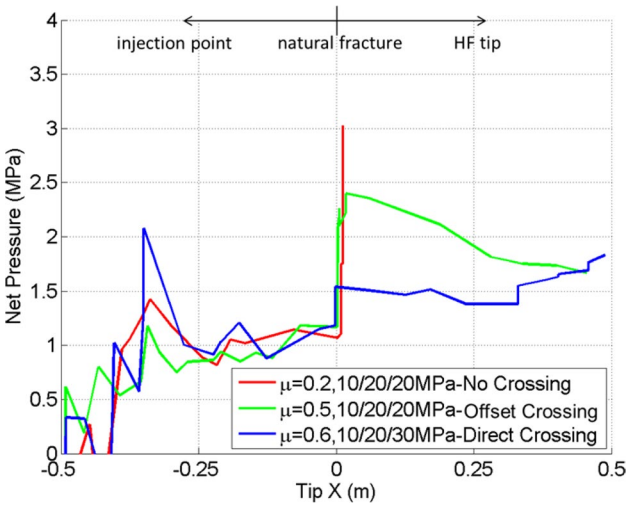

Fig. 9 Net pressure at the inlet of the PFC domain versus the hydraulic fracture tip location for the three representative cases

might indicate the breakthrough crossing of the hydraulic fracture over a natural fracture or an interface.

Figure 10 summarizes the results of 20 orthogonal crossing cases for various stress ratios and friction coefficients of the natural fracture. Each case is identified as one of the three crossing scenarios mentioned above. These 20 cases form a 4×5 matrix in the figure. As the coefficient of friction or the stress ratio increases, the crossing pattern experiences the gradual transition from no crossing, to offset crossing, and then to direct crossing. The simulation results are consistent with the crossing criterion proposed in the literature (e.g., Renshaw and Pollard 1995; Gu et al. 2012).

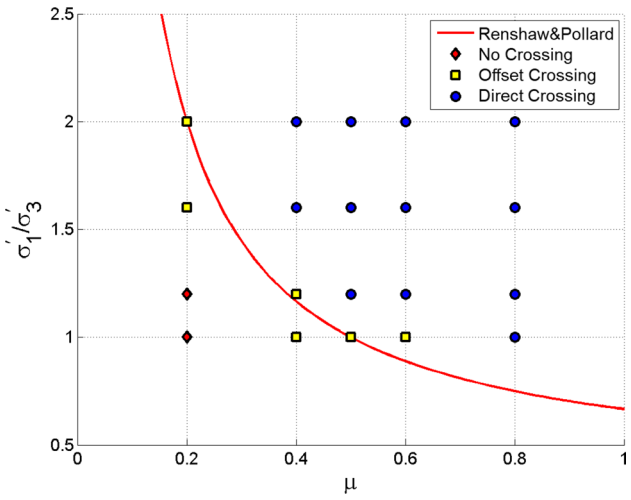

Fig. 10 Results of 20 orthogonal crossing cases for various stress ratios and friction coefficients of the natural fracture; the red line represents the crossing criterion reported in Renshaw and Pollard (1995) (color figure online)

The above analysis focuses on the hydraulic/natural fracture interaction in two-dimensional approximation in which the natural fractures can be simplified as line segments. However, the natural fracture could have a non-orthogonal angle with the hydraulic fracture (Tang et al. 2018), and the existence of the third dimension could make the actual crossing much more complicated (Damjanac and Cundall 2017). Figure 11 shows the simulation results of three-stage interaction between a hydraulic fracture (indicated by green dots) with a pre-existing natural fracture (indicated by red dots) shown in plan-view (*XY* plane). As shown in Fig. 11, the propagation of a horizontal hydraulic fracture is simulated (the vertical stress is the minimum principal stress) by injection of fluid in the vicinity of a vertical penny-shaped, pre-existing fracture in an otherwise homogeneous rock. Three stages of the fracture geometry are present to demonstrate the fracturing evolution process. The hydraulic fracture starts propagating as a penny-shaped fracture. When the hydraulic fracture reaches the pre-existing vertical fracture (Fig. 11a), its propagation in that direction is apparently arrested. Subsequently, the hydraulic fracture continues to propagate on both sides around the pre-existing fracture (Fig. 11b) until the two sides merge, completely enclosing the pre-existing fracture (Fig. 11c). The side-view (*XZ* plane) of the fractures is shown in Fig. 12. It appears that the hydraulic fracture has propagated through the pre-existing fracture. As the three-dimensional model shows, the actual mechanism of hydraulic/natural fracture interaction is very different and cannot be approximated in a two-dimensional model. Thus, a crossing that can be correctly predicted in three-dimensional analysis can be mischaracterized as a complete arrest of hydraulic fracture by a pre-existing natural fracture in two-dimensional approximation.

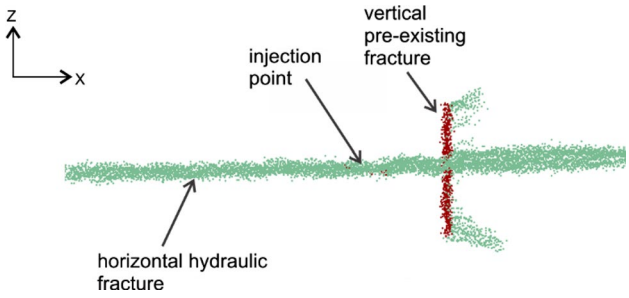

Fig. 12 Side-view (*XZ* plane) of the interaction between a hydraulic fracture (indicated by green dots) with a pre-existing natural fracture (indicated by red dots) after 1500 s of injection (color figure online)

The above analysis indicates that the three-dimensional nature is essential for understanding the hydraulic/natural fracture interaction. In addition, natural fractures in in situ conditions could be either frictional and permeable, or cemented with minerals with varying degrees (Gale et al. 2007, 2014) and impermeable. Laboratory experiments show that these properties greatly influence the crossing behavior (Bahorich et al. 2012; Fu et al. 2016). Although the mechanism of hydraulic/natural fracture interaction is complex, the combination of laboratory experiments with three-dimensional modeling demonstrated in this paper could provide a viable path to solving this challenging problem.

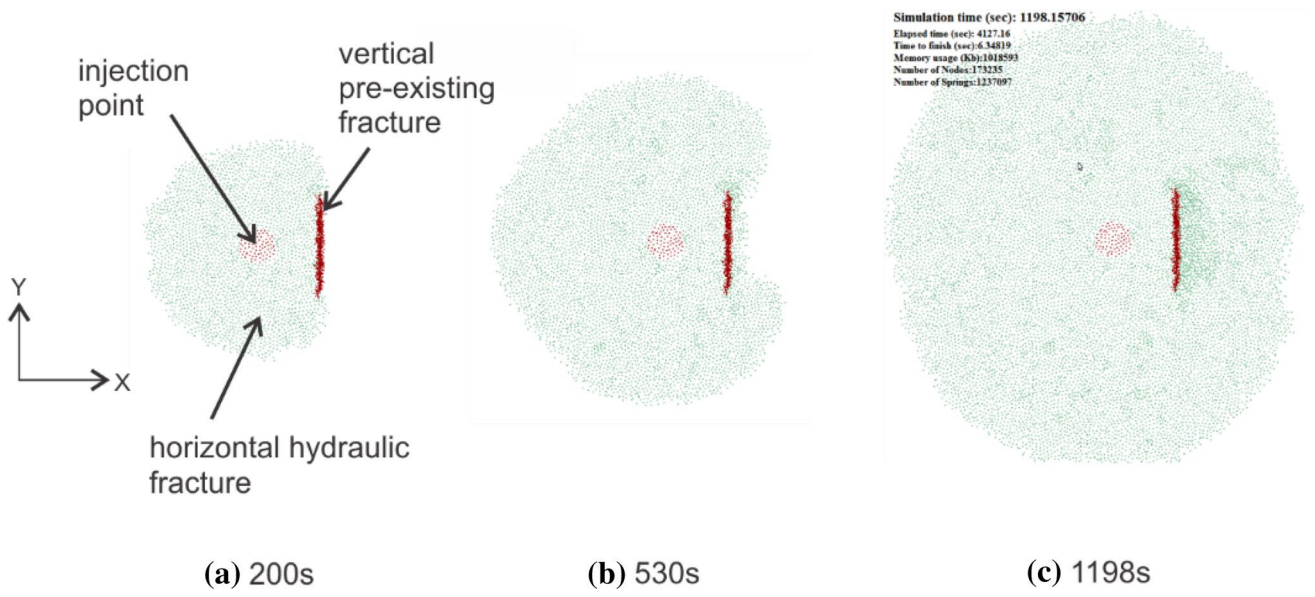

Fig. 11 Three stages of interaction between a hydraulic fracture (indicated by green dots) with a pre-existing natural fracture (indicated by red dots) shown in plan-view (*XY* plane) (color figure online)

5 Multi-Stage Hydraulic Fracturing with DFN

Effective multi-stage hydraulic fracturing stimulation is the key for economic exploitation of unconventional reservoirs. Nevertheless, there is typically limited data available to evaluate the performance of hydraulic fracturing and understand the rock mass response to fluid injection. The pumping pressure history, fluid tracers, tiltmeter monitoring of surface deformation, and microseismicity monitoring are the few techniques that could provide some indirect measurements for fracture diagnosis. Among them, microseismicity is the most common method to "image" the hydraulic fractures. The microseismic data are generated by the instantaneous slip along pre-existing planes of weakness and thus provide information on the location, time, magnitude and source mechanisms of local shearing caused by fluid injection.

Microseismicity and geomechanical modeling can be combined to infer the hydraulic fractures (Haddad et al. 2017). The workflow is shown in Fig. 13. The geological and geomechanical information required to set up the geomechanical models of hydraulic fracturing is typically available and fairly well understood. However, the DFN data include a lot of uncertainty. The fracture network connectivity of a DFN could greatly affect the hydraulic fracture effectiveness and microseismicity generation (Zhang et al. 2013b). Due to the stochastic nature of rock fracturing and limited data on reservoir fracturing characterization, it is practically impossible to create a deterministic DFN model for a reservoir. Microseismic amplitude ratio analysis and moment tensor inversion based on source parameters could help to identify the dominant fracture orientation. Then, a synthetic Microseismic DFN (MSDFN) can be statistically constructed by integrating the microseismic attributes with the well logs (image log of fractures, rock outcrops, etc.). The MSDFN with fracture spacing, orientation, and size is then imported into the SRM model. The models can be calibrated by comparing their results with the observed field microseismicity and the injection pressure history until the predicted and observed data are in good agreement.

A case study following the workflow in Fig. 13 was carried out to calibrate the hydraulic fracturing model for a well located in the Horn River Basin, British Columbia, Canada (Lee et al. 2016; Maxwell et al. 2016). The in situ stress and pore-pressure curve from the wellbore are plotted in Fig. 14. Mechanical properties for the model were derived from well logs in the nearby wells, while the MSDFN was constructed based on the processed microseismic data. The DFN consists of one major set of natural fractures subparallel to the SHmax direction while the fracture dimensions and density are also estimated from the microseismicity. We selected the fifth fracturing stage as the representative stage that has three perforation clusters 25 m apart. A 95 min injection at 9.6 m^3/min rate was simulated.

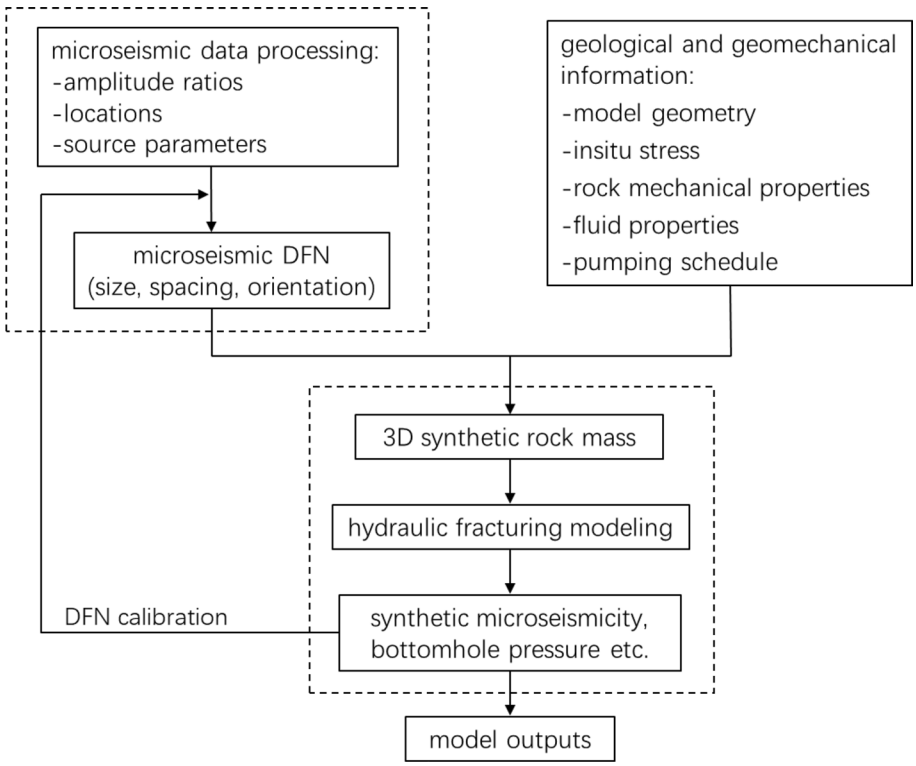

Fig. 13 Calibration of geomechanical models with microseismic data to infer the effect of hydraulic fracturing

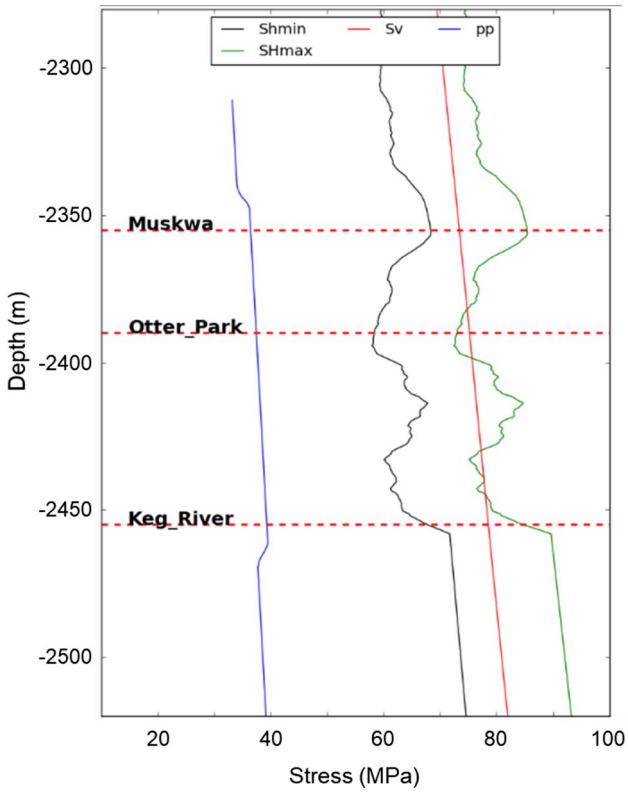

Fig. 14 In situ stress and pore pressure for the model of multi-stage fracturing with DFN

The first step of the calibration is to determine the fracture height and length with consistent distributions of seismic moment with depth and laterally. Figure 15a shows the perspective view of primary fractures and synthetic microseismicity and the light blue rectangles represent the MSDFN. Figure 15b, c plots the comparison of seismic moment release distributions between the model and field observations for both the vertical and lateral directions. The model is expected to produce slightly higher moments than the field data, because the field events are never expected to record all the deformation. A good match is found in terms of the span and distribution of the microseismic moment for both the vertical and lateral directions.

In addition, Fig. 16 shows the map view of the simulated microseismicity in the model (white dots) and recorded microseismicity in the field (green dots). The light green rectangles in the plot represent the MSDFN. The results show that not only the extent of the microseismicity but also the general character of the microseismicity is representative, which suggests that the geomechanical model is well calibrated. Note that in the microseismic comparison, modeled locations have been statistically perturbed based on the reported location accuracy of the field data. This has the effect of spreading the events out, consistent with the resolution of the real microseismic image.

The aperture contours of the primary fracture planes for the three clusters are plotted in Fig. 17. The three primary fractures have similar heights and lengths, but the hydraulic fracture from the central cluster has a slightly smaller aperture and grows in the opposite direction from the other two due to the stress-shadowing effect. The proppant distribution on the primary fracture planes is plotted in Fig. 18. Except for some small screen-out area near the tip, the distribution of proppant in general follows the fracture profile shown in Fig. 17.

A calibrated model is the starting point for parametric studies and hydraulic fracturing optimization. The production and reservoir drainage can be estimated from a calibrated fracture model by performing a reservoir simulation using enhanced permeability as a function of the proppant concentration. Alternatively, the product of the fracture surface contact area and some reservoir quality metric (e.g., hydrocarbon pore volume) can be used to compare different completion designs. Proppant concentration thresholds can also be used to identify the propped portion of the fracture to limit the effective fracture area to where the permeability would be enhanced. Different fracture designs (e.g., rate, fluid type, and proppant schedule) can be compared

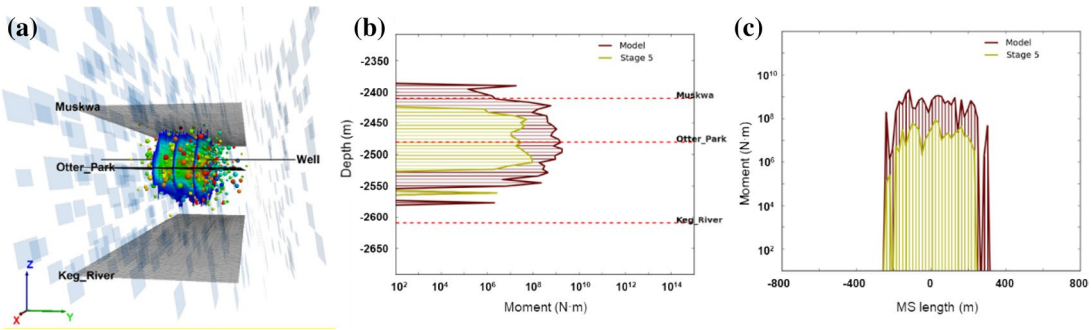

Fig. 15 **a** Perspective view of primary fractures and synthetic microseismicity; the light blue rectangles represent the MSDFN; **b** depth distribution of microseismic moment release from the model (red) and observed (green); and **c** lateral distribution of microseismic moment release from the model and observed (Lee et al. 2016; Maxwell et al. 2016) (color figure online)

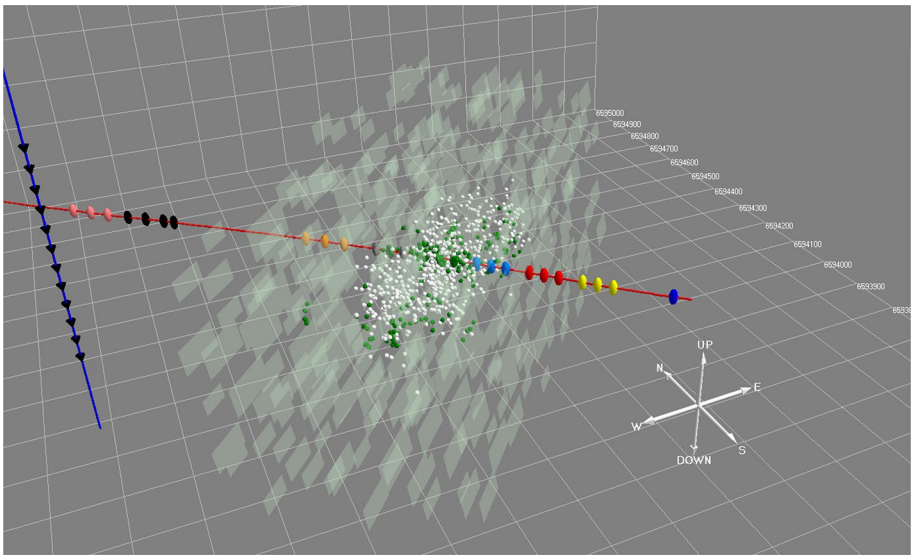

Fig. 16 Map view of the simulated microseismicity in the model (white dots) and recorded microseismicity in the field (green dots). The light green rectangles represent the MSDFN (color figure online)

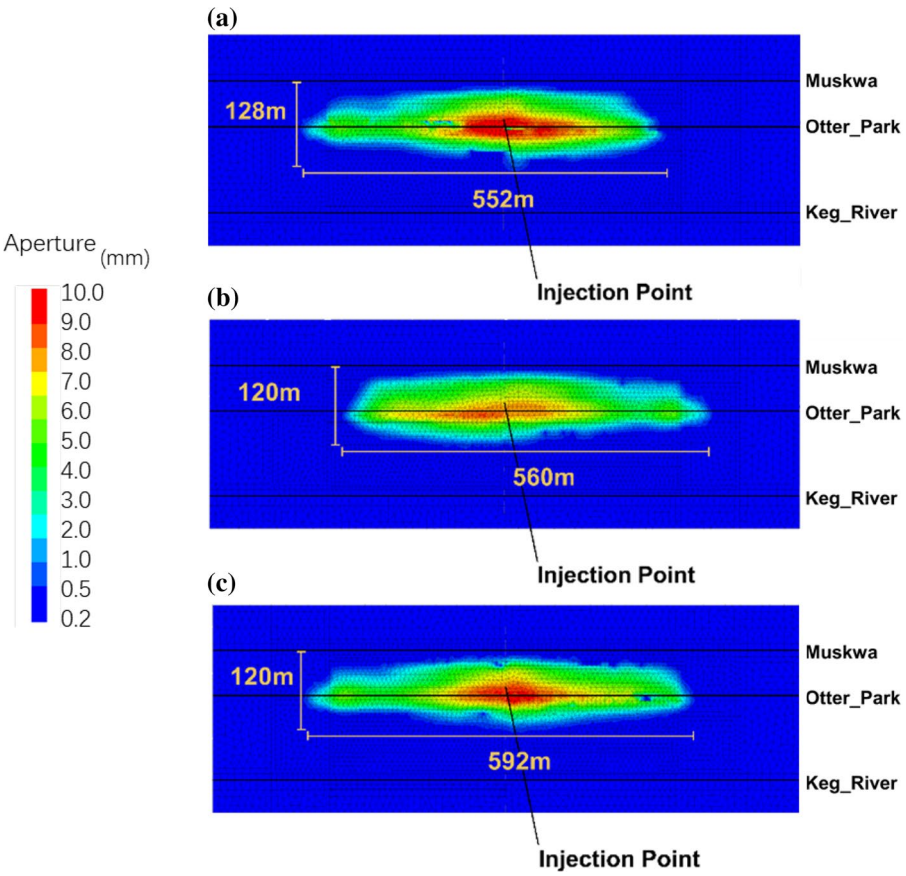

Fig. 17 Aperture of the primary fracture planes for the three clusters

to optimize the reservoir contact in the zone of influence and guide the field operations. The well completion (e.g., number of perforation clusters and spacing) can be tested to investigate the potential impact of stress shadowing between competing adjacent fractures, along with potential well orientations to examine the impact of offset fracture initiation points relative to the stress field. The landing depth of the horizontal wells can be investigated to maximize contact with the zone of interest. Similarly, well spacing can be investigated, including the effective drainage offset from each lateral and potential hydraulic and mechanical interference during fracturing. The model described here is 3D and

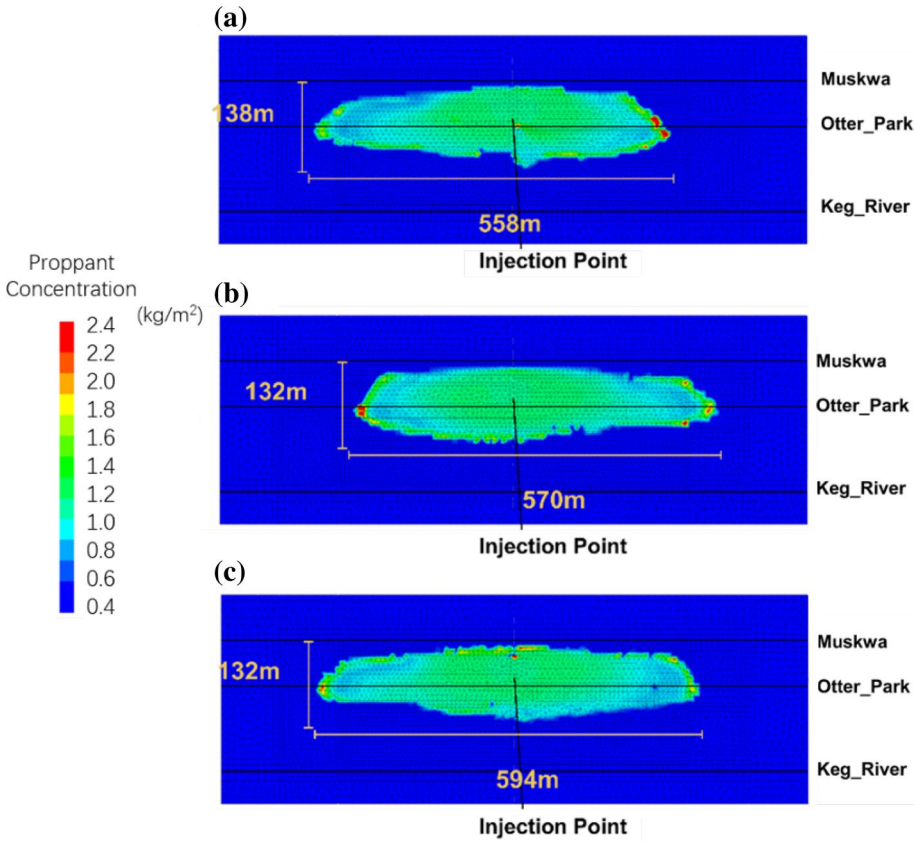

Fig. 18 Proppant distribution on the primary fracture planes for the three clusters

so the optimal well sequencing between laterals in different zones can also be explored. In summary, the case study here demonstrates the quantitative use of microseismicity to inform and calibrate the geomechanical modeling, which not only enhances the understanding and value of monitoring data by integrating geomechanics into the interpretation, but also increases the confidence in geomechanical modeling by ensuring consistency with field diagnostics.

6 In-Fill Well Fracturing After Depletion-Induced Stress Change

In-fill well fracturing has become a frequent and common operation in the oil and gas industry for unconventional resource recovery. One of the key factors that affects the in-fill well fracturing treatment is the altered reservoir pressure and stress around previously produced wells. Since the parent well has experienced some period of depletion when the new in-fill well is drilled and fractured, the reservoir pressure could be largely reduced compared with the original in situ value (Singh et al. 2008; Safari et al. 2017; Guo et al. 2018). The decrease of reservoir pressure could cause the reduction and the reorientation of principal stresses as suggested by the Biot theory (Biot 1956; Detournay and Cheng 1993). Since local alteration of stresses can significantly affect the propagation of hydraulic fractures (Roussel et al. 2013; Zhang and Mack 2017; Zhang and Dontsov 2018), the timing and spacing of in-fill well are of great importance to control the overall of effectiveness of in-fill well treatments.

We applied a multiscale modeling strategy to study the depletion-induced stress change and in-fill well fracturing at both the well and stage scale for the Bakken Shale (Mack et al. 2016; Dohmen et al. 2017). The geometry of parent and in-fill wells for the case study is shown in Fig. 19. The detailed input parameters for this model can be found in Table 3. A total of four wells are shown in the plot, including one parent well and one observation well in the middle, and two in-fill wells on the two sides. A 14-stage initial hydraulic fracture treatment was performed for the parent well, with each stage including four perforation clusters. The parent well produced for approximately 2.5 years prior to the completion of two in-fill wells. The two red dots in Fig. 19 indicate the injection points of two representative fracturing stages from the two in-fill wells, while the yellow and green dot clouds of microseismicity indicate the asymmetric propagation of hydraulic fractures toward the parent well.

Well-scale geomechanical modeling was first performed to estimate the stress response due to the depletion around the parent well. The initial fracture treatment in the parent well had been simulated independently and had been idealized in reservoir simulations as a set of 56 planar

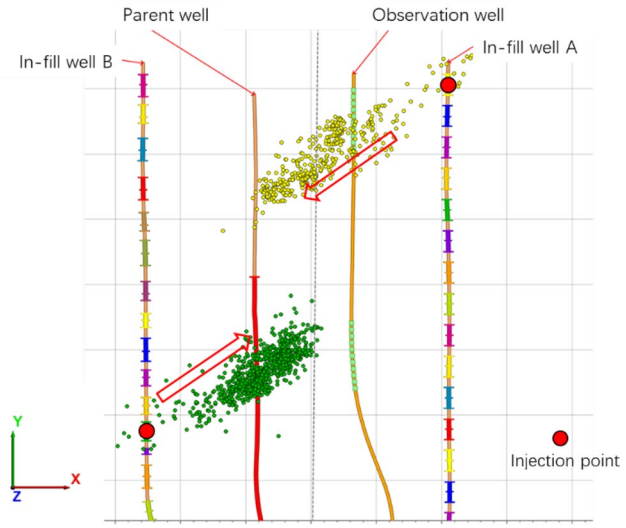

Fig. 19 Geometry of parent and in-fill wells for the case study in Bakken shale; the two red dots indicate the injection points of two fracturing stages from the two in-fill wells, while the yellow and green dot clouds of microseismicity indicate the asymmetric propagation of hydraulic fractures (color figure online)

Table 3 Input parameters in the infill well fracturing model

Well information	
Well spacing (m)	~230
Horizontal leg (m)	~1500
Depth (m)	3383.3
Stress and pore pressure	
SH_{min} gradient (kPa/m)	17.8
SH_{max} gradient (kPa/m)	21.3
Sv gradient (kPa/m)	23.7
PP gradient (kPa/m)	15.4
Depletion parameters	
Bottomhole pressure (MPa)	13.8
Biot's coefficient	0.5

fractures (14 stages, each with 4 clusters) oriented parallel to the initial maximum horizontal stress. The geometry of the well-scale geomechanical model is shown in Fig. 20. The depleted pressure field from the reservoir simulator (Fig. 21a) was exported to the well-scale geomechanical model to calculate the resulting minimum horizontal stress and orientation of maximum horizontal stress (Fig. 21b, c). Note that the initial maximum stress (SHmax) in this area is oriented 55° from north. Depletion around wells oriented north–south thus causes a change in the orientation of the horizontal stresses of up to ± 10° near the wellbore, resulting in induced shear stress on the hydraulic fractures.

The stresses from the well-scale simulation were used as boundary and initial conditions for a more detailed stage-scale simulation of in-fill well fracturing (Fig. 22). The pore pressure and stress in the well-scale model were output first and then input into the stage-scale model through grid-to-grid interpolation. The pre-existing natural fracture network was represented by a hypothetical DFN (blue segments in Fig. 22b) with a few fractures parallel and perpendicular to the hydraulic fracture planes. The red dot represents the injection point of the simulated stage for the in-fill well fracturing.

Figure 23 shows the modeled microseismic activity during in-fill well fracturing at different injection times for a total of 280 min of injection. The background color indicates the pore pressure due to the depletion of the parent well, and the color of the microseismicity (spheres in the plot) indicates the timing of the injection. The simulation results in Fig. 23 predict that the offset well fracture would propagate very asymmetrically toward the parent well, consistent with the field observation shown in Fig. 19. Note that the initial synthetic microseismic response is symmetric, but by the end of the treatment, it becomes very asymmetric, suggesting that the asymmetry observed in the field data is not caused by distance bias or other microseismic acquisition and processing limitations.

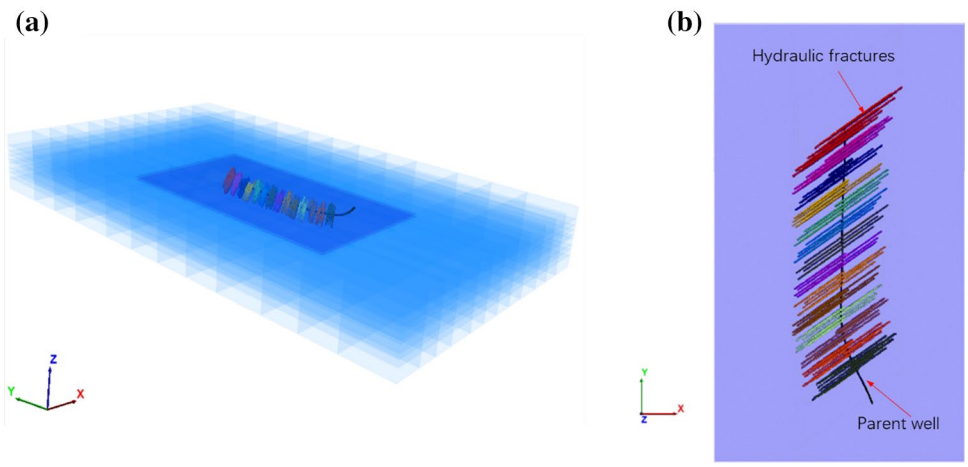

Fig. 20 Well-scale geomechanical model for stress calculation after depletion of the parent well: **a** perspective view of the 3D model; and **b** top view (*XY* plane) of the parent well with 56 planar hydraulic fractures

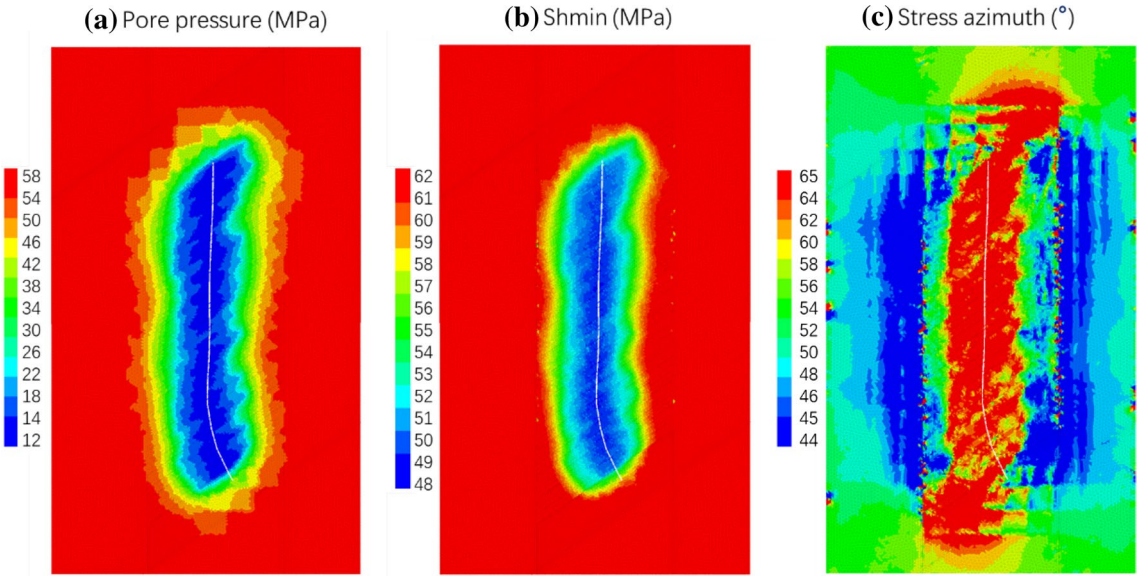

Fig. 21 **a** Pore pressure from reservoir simulator due to the depletion of the parent well; **b** resulting minimum horizontal stress calculated by geomechanical modeling; and **c** resulting orientation of maximum horizontal stress after depletion showing rotations of up to ± 10° from the undepleted state

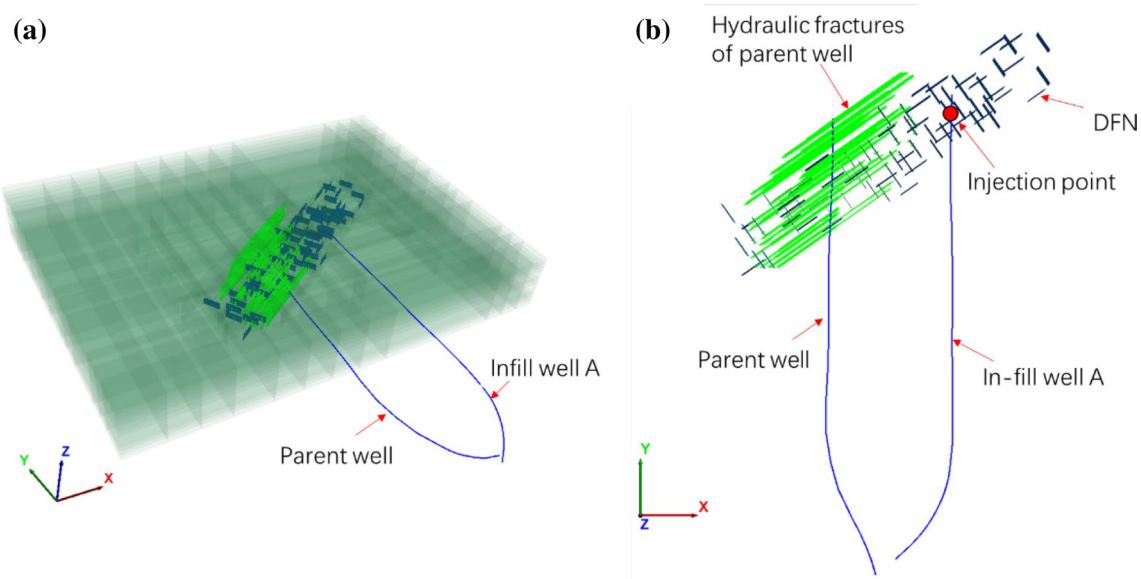

Fig. 22 Stage-scale geomechanical model for in-fill well fracturing: **a** perspective view of the 3D model; and **b** top view (*XY* plane) of the geometry of parent well and in-fill well. The green planes are the initial hydraulic fractures of parent well and the blue segments represent the DFN in the rock mass

In the field, the pressure increases were detected in the parent well due to "frac hits" from the in-fill well fracturing, indicating that a hydraulic connection was created between the two wells. The pressure increase started after pumping into the in-fill well, consistent with the time it would take for the hydraulic fracture to propagate through the rock, intersect the parent well, and create the connection. The pressure subsequently decreased starting shortly after pumping ended, as shown for one stage of fracturing in Fig. 24a. It should be noted that the time delay before the pressure started to rise and the magnitude of the pressure increase varied among different fracturing stages. In addition, the pressure drop after each stage was smaller than the pressure increase during pumping. As a

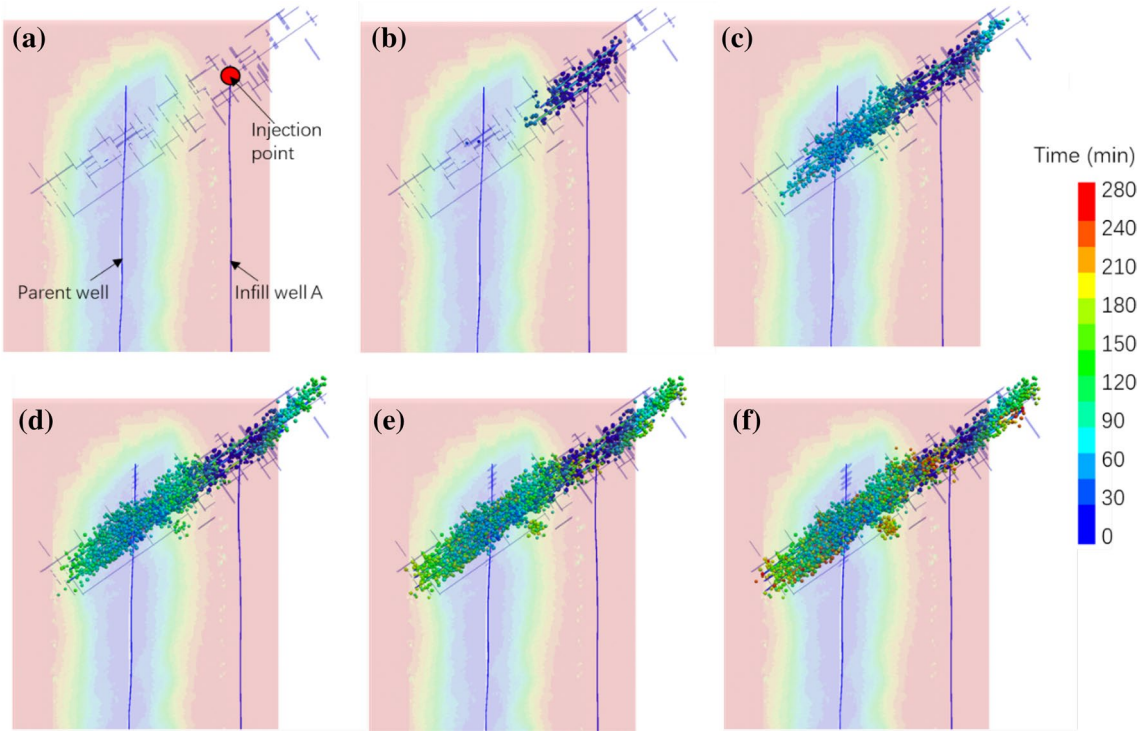

Fig. 23 Model microseismic activity during in-fill well fracturing at different injection times: **a** 0 min; **b** 30 min; **c** 90 min; **d** 150 min; **e** 210 min; and **f** 280 min. The background color indicates the pore pressure due to the depletion of the parent well, and the color of the microseismicity indicates the timing of the injection (color figure online)

result, there was a net increase of pressure in the parent well after each stage.

The frac hits and well interference are modeled with the stage-scale model by the following procedure. First, the magnitude of the pressure increase was calibrated using the field re-pressurization data, which were obtained from the test of slow injection in the parent well to estimate the amount of fluid required to leak into the wellbore of the parent well to generate the pressure change observed in the field. Then, after the hydraulic fracture initiated from the in-filled well reaches the parent well, a certain amount of flow rate is removed from this hydraulic fracture and evenly distributed into the 14 stages of the parent well, assuming that all stages in the parent well are similar and there is no wellbore friction due to the slow flow rate. The model pressure in the parent well calculated for one stage of in-fill well fracturing is shown in Fig. 24b, compared with two typical stages of the field data. Note that the volume needed to pressurize the parent well is very small (less than 2% of the fluid pumped) and has no significant effect on the in-fill well fracture geometry or pressure.

In summary, production after the original hydraulic fracture treatments can alter both the local pore pressure and the stress field around the depleted zones. Understanding these changes is important for designing the refracturing and in-fill well fracturing to properly target undepleted portions of the reservoir. From the perspective of numerical modeling, these results clearly indicate the requirement of accurately accessing the pore pressure and stress fields before the refracturing modeling. Also, the pressure and stress heterogeneity in the simulation domain need to be accounted for when modeling the hydraulic fracture propagation of the in-fill wells.

7 Induced Seismicity Associated with Fault Reactivation

In recent years, the impact of hydraulic fracturing on the environment has raised great public concerns (Jackson et al. 2014). Induced seismicity due to fluid injection is one of the major concerns (Ellsworth 2013; van der Elst et al. 2013; McGarr 2014; Bao and Eaton 2016; Rubinstein et al. 2018). Both hydraulic fracturing and the reinjection of co-produced waste water have been proven to cause induced seismicity (Elsworth et al. 2016). Those concerns result in the development of industry protocols such as the traffic-light systems based on seismic monitoring to mitigate seismic hazard (Maxwell 2014). Quantitative geomechanical assessment can model pore-pressure diffusion and mechanical stresses/strains associated with hydraulic fracture treatments, and thus can be used to improve the understanding of fault reactivation and corresponding seismic response.

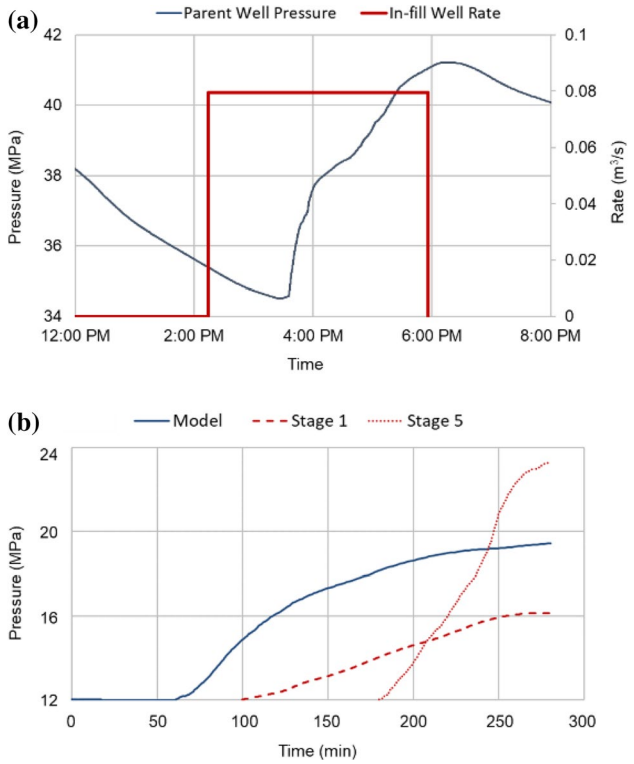

Fig. 24 **a** Field data of injection rate (red thick line) in in-fill well and wellbore pressure (blue thin line) in parent well showing delayed frac hits, and **b** parent wellbore pressure in the model (solid line) and two representative stages in the field (dotted lines) (color figure online)

3D distinct-element modeling was applied to assess the seismic hazard associated with hydraulic fracturing based on the published case in the Horn River basin (Maxwell et al. 2015c; Zhang et al. 2015). Field microseismic data clearly show lineation of relatively large microseismic events (pointed by red arrows in Fig. 25a) caused by fault reactivation (Snelling and de Groot 2014). Those events are not sufficiently large to be felt on the surface (i.e., $M_w > 3.0$) but could be easily separated with other hydraulic fracturing related events. Figure 25b shows the schematic of three different modeling scenarios of fault and hydraulic fracture interaction. Different relative positions of a fault and hydraulic fractures (Cases 1, 2, and 3) are analyzed in the geomechanical model. The model considers one hydraulic fracturing stage with five perforation clusters along the horizontal well, each with a potential planar hydraulic fracture orthogonal to the well. A strike–slip stress regime is applied in the model. The fault has a dip of 90° and intersects the horizontal well at 45°. Detailed model parameters are summarized in Table 4. In Case 1, no direct interaction between the fault and the planar hydraulic fractures is expected, although the total stress changes still could cause the fault to slip. In Case 2, the fault is intersected with two hydraulic fractures, and in Case 3, the fault is designed to be intersected with all five hydraulic fractures.

In this study, the non-linear softening–healing Coulomb slip model was applied to simulate the mechanical behavior of the fault (Fig. 26). Compared with the classic Coulomb slip model, two major improvements were made in the non-linear softening–healing Coulomb slip model: first, when the fault starts to slip, the friction angle evolves from the peak value of $\emptyset_{peak}$ to the residual value of $\emptyset_{resid}$ over a specified critical slip distance D_c; second, the shear strength recovers instantaneously to the peak value when the slipping stops.

Figures 27, 28, and 29 show the fracture aperture, pore pressure, shear displacement, and estimated synthetic microseismicity for Cases 1, 2 and 3, respectively. In Case 1, only the leftmost and rightmost hydraulic fractures fully develop into bi-wing fractures. The three hydraulic fractures in the

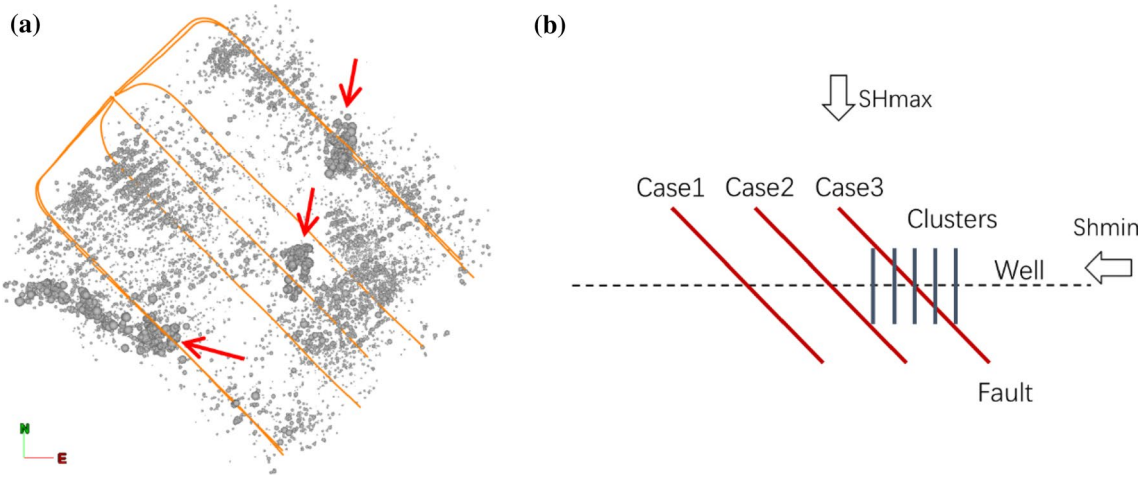

Fig. 25 **a** Processed field microseismic data; the red arrows show the lineation of activated faults (Snelling and de Groot 2014), and **b** schematic of three different modeling scenarios of fault and hydraulic fracture interaction (color figure online)

Table 4 Input parameters in the fault reactivation model

Rock property	
Elastic modulus (GPa)	39.6
Poisson's ratio	0.221
Fault property	
Normal stiffness (GPa/m)	141.0
Shear stiffness (GPa/m)	70.7
Fault tensile strength (MPa)	0.0
Cohesion (MPa)	0.0
Coefficient of friction	0.577
Dip (°)	90
Dip direction (°)	45
Initial aperture (mm)	0.01
Stress and pore pressure	
SHmin gradient (kPa/m)	21.5
SHmax gradient (kPa/m)	36.0
Sv gradient (kPa/m)	25.2
PP gradient (kPa/m)	12.0
Injection parameters	
Injection rate (m^3/s)	0.25
Fluid viscosity (cp)	20

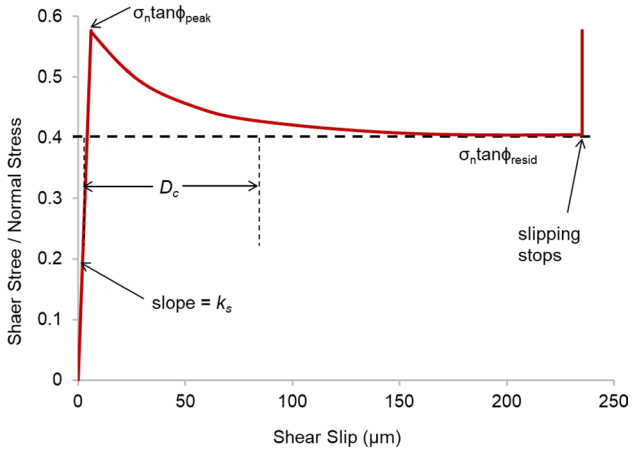

Fig. 26 Non-linear softening–healing Coulomb slip model for the fault

middle are constrained due to the stress shadow effect. The calculated shear displacement indicates that the fault plane experiences no shear displacement, and therefore, no seismicity activity is expected along the fault plane. In Cases 2 and 3, the hydraulic fractures are arrested once they intersect the fault plane, and fracturing fluid is diverted into the fault causing its dilation and slippage. The estimated synthetic microseismicity shows a lineation of relatively large microseismic events along the fault plane. Microseismicity on the natural fractures is relatively small. Note that some remote "dry" microseismicity on the natural fractures also occurs due to the total stress effect (Maxwell et al. 2015a).

Figure 30 shows the cumulative frequency vs. moment magnitude for the three geomechanical modeling cases, indicating larger estimated magnitudes with reactivation of the fault. The three cases are reasonably consistent with the expected power law relationship (Gutenberg and Richter 1942) typical for real microseismic data. In this example, the models have not been adjusted to match the microseismic monitoring, for example, by changing the DFN density and orientation, frictional characteristics, or principal stress magnitudes. However, the modeling is consistent with the elevated magnitudes along the fault in Fig. 25a.

This case study demonstrates the capability of applying a geomechanical model to assess the interaction of hydraulic fractures with faults. The results show that the fault reactivation in the analyzed case only occurs when the hydraulic fractures propagate and intersect the fault, and the pressure increase triggers fault slip and seismic events. Microseismicity predicted by a geomechanical model not only improves the interpretation of the microseismic image but also provides better understanding of the geomechanical response of the reservoir. The methodology thus can complement the monitoring-based traffic-light systems and provide a versatile testing tool for various operational changes to identify a scenario that reduces the seismic hazard associated with hydraulic fracturing.

8 Concluding Remarks

Naturally fractured rock mass is highly inhomogeneous and contains geological discontinuities at various length scales. Hydraulic fracture stimulation in such a medium could result in complex fracture systems instead of simple planar fractures. In this study, we carried out fully coupled multiscale numerical analyses to investigate some key coupled processes of fluid-driven fracture propagation in a naturally fractured rock mass. The numerical analysis follows the concept of the synthetic rock mass (SRM) model initially developed in discrete element method (DEM). We introduce a total of five case studies, including fracture initiation and near wellbore tortuosity, hydraulic fracture interaction with natural fractures, multi-stage hydraulic fracturing with discrete fracture network (DFN), depletion-induced stress change and in-fill well fracturing, and fault reactivation and induced seismicity.

The main conclusions of this study are as follows:

- Fracture initiation and near wellbore tortuosity are complex multiscale problems. 3D non-planar mixed-mode fracture propagation criterion, explicit modeling of borehole and perforation tunnels, and the stress redistribution

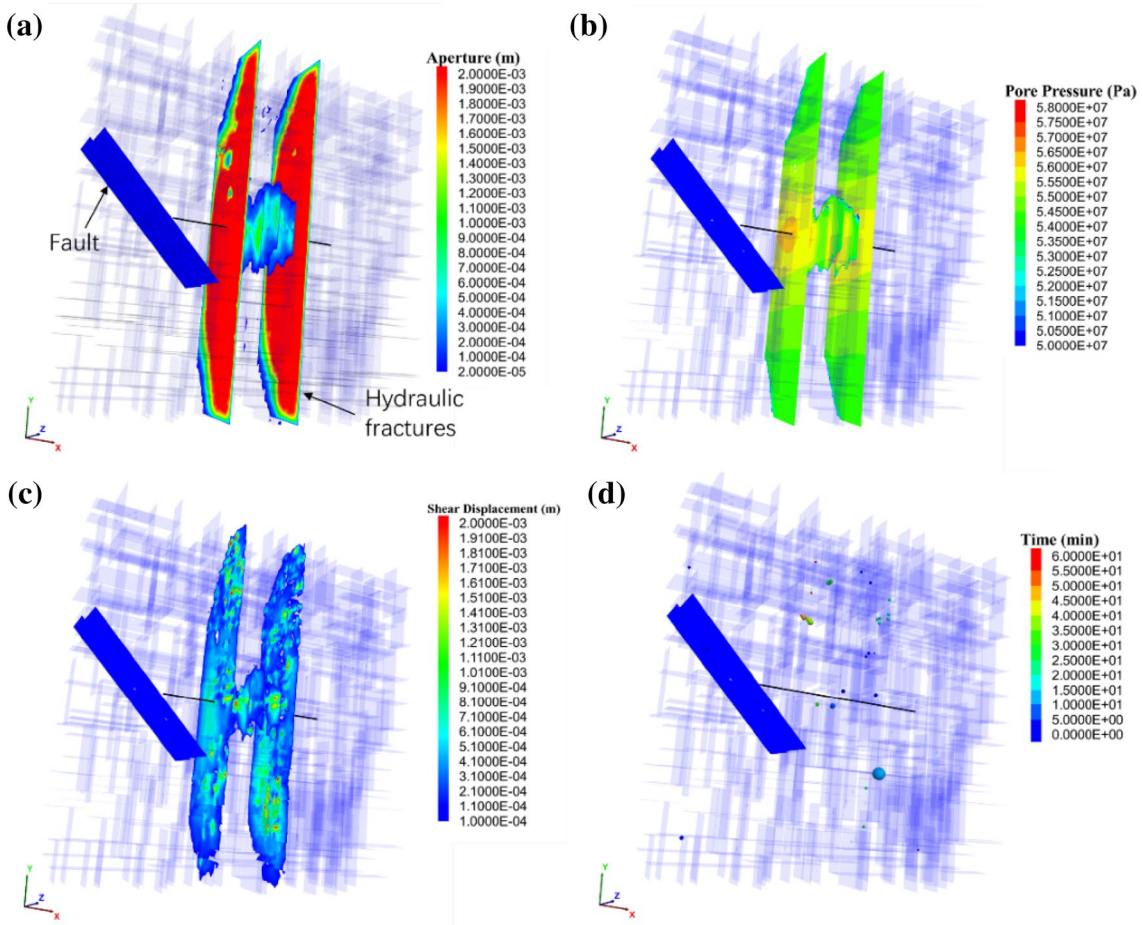

Fig. 27 Geomechanical modeling results of Case 1: **a** the fracture aperture; **b** the pore-pressure contours; **c** the shear displacements contours; and **d** the estimated synthetic microseismicity

due to the construction of borehole and perforations are required in the numerical modeling to investigate the basic mechanism.

- Natural fractures greatly influence the propagation of hydraulic fractures. Characterization of the natural fracture properties and the three-dimensional nature of the problem are essential to minimize the uncertainties and help better understand the mechanism of hydraulic–natural fracture interaction.
- A workflow of modeling hydraulic fractures is presented. It includes quantitatively applying microseismicity to generate the MSDFN and calibrate the geomechanical model. The calibrated geomechanical model can be used in parametric studies and hydraulic fracturing optimization.
- Production after the original hydraulic fracture treatments can alter both the local pore pressure and the stress fields. Accessing to accurate pore pressure and stress fields before the refracturing modeling is critical. The pressure and stress heterogeneities need to be accounted for when modeling the in-fill well fracturing.
- The interaction between hydraulic fractures and pre-existing faults can be assessed by employing a microseismic calculated from the geomechanical models. The methodology provides a versatile testing tool for various operational changes to identify a scenario that reduces the seismic hazard associated with hydraulic fracturing.

Through those case studies, we demonstrate that with an advanced numerical modeling tool, the complex fracturing associated with hydraulic fracturing in a naturally fractured rock mass can be quantitatively analyzed and the extent of various uncertainties can be assessed. Note that the term "fully coupled" in this paper is only applicable to single

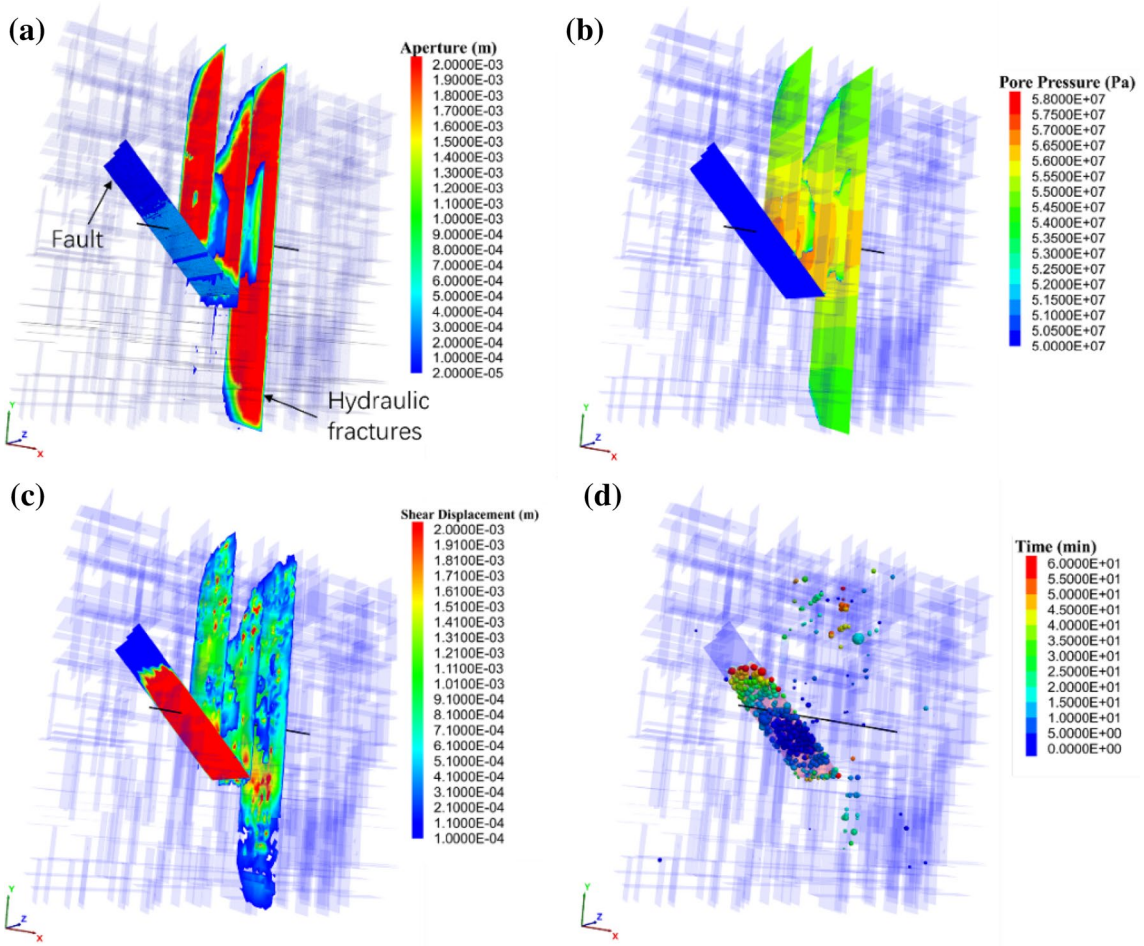

Fig. 28 Geomechanical modeling results of Case 2: **a** the fracture aperture; **b** the pore-pressure contours; **c** the shear displacement contours; and **d** the estimated synthetic microseismicity

occasion of hydraulic fracturing, depletion, and refracturing. The cases of in-fill well fracturing or refracturing may require the sequential modeling of depletion and fracturing. However, it can still be claimed that at each step, e.g., depletion or fracturing, the numerical modeling is fully coupled.

It should be mentioned that although numerical analysis is probably the most powerful tool to analyze complex problems such as hydraulic fracturing in naturally fracture rock masses, it is still an approximation of the real physical process. With different assumptions, even for the same engineering problem, different numerical schemes might not give the exact same results. Given the levels of complexity, the numerical analysis, hence, should not be taken as the absolute answer of those challenging problems discussed in this paper, but it provides important insights of the controlling behaviors.

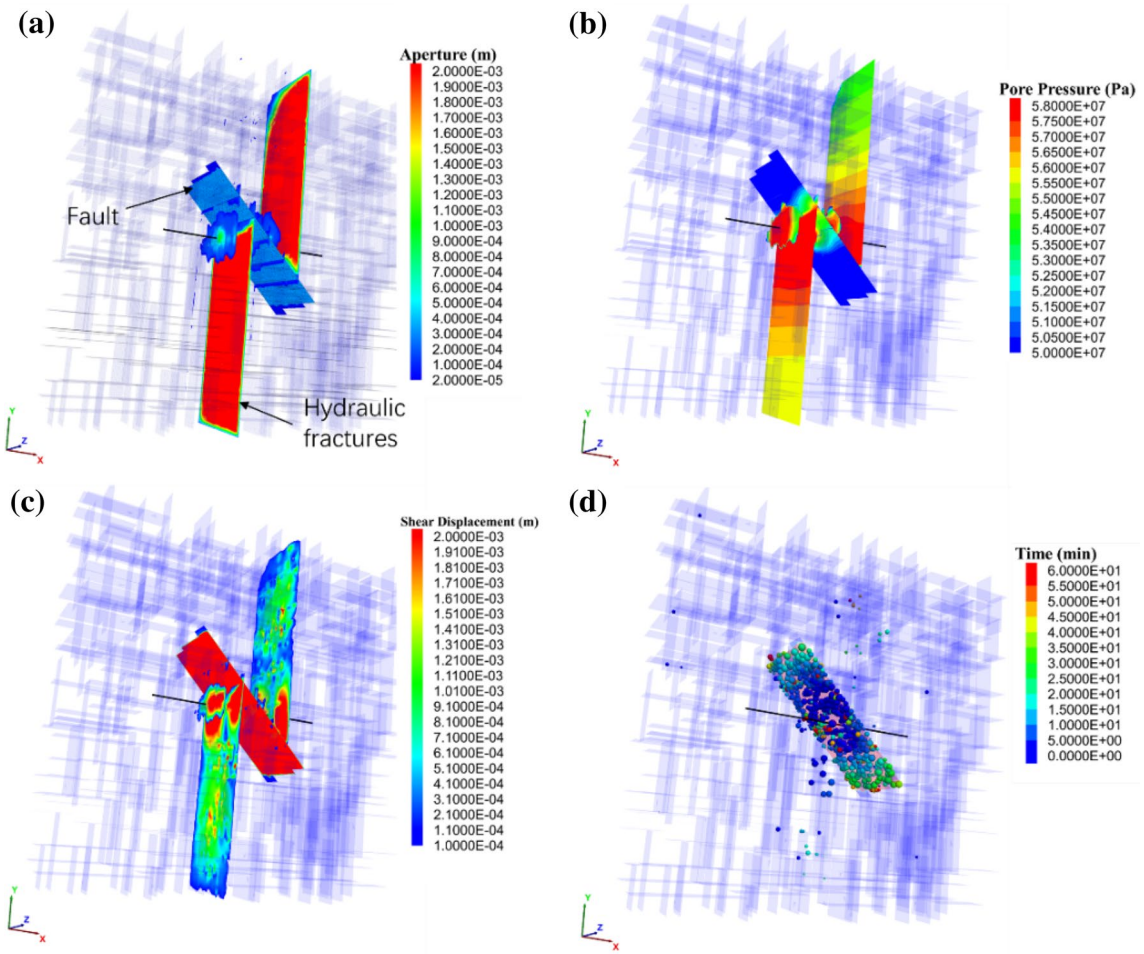

Fig. 29 Geomechanical modeling results of Case 3: **a** the fracture aperture; **b** the pore-pressure contours; **c** the shear displacement contours; and **d** the estimated synthetic microseismicity

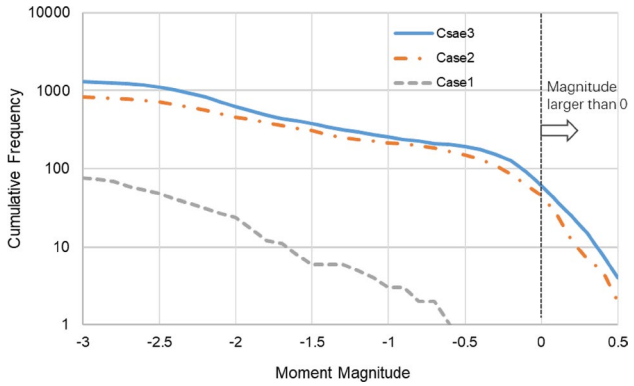

Fig. 30 The cumulative frequency vs. moment magnitude for the three geomechanical modeling cases

Acknowledgements This paper was prepared based on the 2018 ARMA Early Career Keynote Lecture delivered by the first author, FZ. The authors would like to thank ARMA for the invitation of preparing this keynote paper. FZ acknowledges the financial support by the National Key R&D Program of China (2017YFC1500703), the National Natural Science Foundation of China under grant 41772286 and PetroChina Innovation Foundation under grant 2018D-5007-0202. We thank guest editor Richard Schulz and an anonymous reviewer for the insightful comments which help to improve the paper.

References

Adachi J, Siebrits E, Peirce A, Desroches J (2007) Computer simulation of hydraulic fractures. Int J Rock Mech Min Sci 44:739–757. https://doi.org/10.1016/j.ijrmms.2006.11.006

Advani SH, Torok JS, Lee JK, Choudhry S (1987) Explicit time-dependent solutions and numerical evaluations for penny-shaped hydraulic fracture models. J Geophys Res 92:8049–8055. https://doi.org/10.1029/JB092iB08p08049

Advani SH, Lee TS, Lee JK (1990) Three-dimensional modeling of hydraulic fractures in layered media: part I—finite element formulations. J Energy Resour Technol 112:1–9. https://doi.org/10.1115/1.2905706

Aimene YE, Ouenes A (2015) Geomechanical modeling of hydraulic fractures interacting with natural fractures—validation with microseismic and tracer data from the Marcellus and Eagle

Ford. Interpretation 3:SU71–SU88. https://doi.org/10.1190/int-2014-0274.1
Bahorich B, Olson JE, Holder J (2012) Examining the effect of cemented natural fractures on hydraulic fracture propagation in hydrostone block experiments. In: SPE Annual Technical Conference and Exhibition
Bao XW, Eaton DW (2016) Fault activation by hydraulic fracturing in western Canada. Science (80-) 354:1406–1409. https://doi.org/10.1126/science.aag2583
Barenblatt GI (1962) The mathematical theory of equilibrium cracks in brittle fracture. Adv Appl Mech 7:55–129. https://doi.org/10.1016/S0065-2156(08)70121-2
Bažant ZP, Salviato M, Chau VT et al (2014) Why fracking works. J Appl Mech 81:101010. https://doi.org/10.1115/1.4028192
Biot M (1956) General solutions of the equation of elasticity and consolidation for a porous material. J Appl Mech 23:91–96
Carrier B, Granet S (2012) Numerical modeling of hydraulic fracture problem in permeable medium using cohesive zone model. Eng Fract Mech 79:312–328. https://doi.org/10.1016/j.engfracmech.2011.11.012
Carter BJ, Desroches J, Ingraffea AR, Wawrzynek PA (2000) Simulating fully 3D hydraulic fracturing. Wiley Publishers, New York
Chen Z, Bunger AP, Zhang X, Jeffrey RG (2009) Cohesive zone finite element-based modeling of hydraulic fractures. Acta Mech Solida Sin 22:443–452. https://doi.org/10.1016/S0894-9166(09)60295-0
Clifton RJ, Abou-Sayed AS (1981) A variational approach to the prediction of the three-dimensional geometry of hydraulic fractures. In: SPE/DOE Low Permeability Gas Reservoirs Symposium
Dahi Taleghani A, Gonzalez M, Shojaei A (2016) Overview of numerical models for interactions between hydraulic fractures and natural fractures: challenges and limitations. Comput Geotech 71:361–368. https://doi.org/10.1016/j.compgeo.2015.09.009
Damjanac B, Cundall P (2016) Application of distinct element methods to simulation of hydraulic fracturing in naturally fractured reservoirs. Comput Geotech 71:283–294. https://doi.org/10.1016/j.compgeo.2015.06.007
Damjanac B, Cundall PA (2017) Effect of jointing and initial stress state on coupled hydro-mechanical processes in rock masses. Hydraul Fract J 4:1–18
Damjanac B, Detournay C, Cundall PA (2016) Application of particle and lattice codes to simulation of hydraulic fracturing. Comput Part Mech 3:249–261. https://doi.org/10.1007/s40571-015-0085-0
Davy P, Le Goc R, Darcel C et al (2010) A likely universal model of fracture scaling and its consequence for crustal hydromechanics. J Geophys Res Solid Earth 115:B10411. https://doi.org/10.1029/2009JB007043
Deng JQ, Lin C, Yang Q et al (2016) Investigation of directional hydraulic fracturing based on true tri-axial experiment and finite element modeling. Comput Geotech 75:28–47. https://doi.org/10.1016/j.compgeo.2016.01.018
Detournay E (2004) Propagation regimes of fluid-driven fractures in impermeable rocks. Int J Geomech 4:35–45. https://doi.org/10.1061/(ASCE)1532-3641(2004)4:1(35)
Detournay E (2016) Mechanics of hydraulic fractures. Annu Rev Fluid Mech 48:311–339. https://doi.org/10.1146/annurev-fluid-010814-014736
Detournay E, Cheng A (1993) Fundamentals of poroelasticity. Comprehensive rock engineering. Pergamon Press, Oxford, pp 113–169
Dohmen T, Zhang J, Barker L, Blangy JP (2017) Microseismic magnitudes and *b*-values for delineating hydraulic fracturing and depletion. SPE J 22:1624–1634. https://doi.org/10.2118/186096-pa
Dontsov EV, Zhang F (2018) Calibration of tensile strength to model fracture toughness with distinct element method. Int J Solids Struct 144–145:180–191. https://doi.org/10.1016/j.ijsolstr.2018.05.001
Economides M, Nolte K (2000) Reservoir stimulation, 3rd edn. Wiley, New York
Ellsworth WL (2013) Injection-induced earthquakes. Science (80-) 341:142
Elsworth D, Spiers CJ, Niemeijer AR (2016) Understanding induced seismicity. Science (80-) 354:1380–1381
Fairhurst C (2013) Fractures and fracturing: hydraulic fracturing in jointed rock. Effective and sustainable hydraulic fracturing. International Society for Rock Mechanics and Rock Engineering, Brisbane, pp 47–79
Fu W, Ames BC, Bunger AP, Savitski AA (2016) Impact of partially cemented and non-persistent natural fractures on hydraulic hracture propagation. Rock Mech Rock Eng 49:4519–4526. https://doi.org/10.1007/s00603-016-1103-0
Gale JFW, Reed RM, Holder J (2007) Natural fractures in the Barnett Shale and their importance for hydraulic fracture treatments. Am Assoc Pet Geol Bull 91:603–622. https://doi.org/10.1306/11010606061
Gale JFW, Laubach SE, Olson JE et al (2014) Natural fractures in shale: a review and new observations. Am Assoc Pet Geol Bull 98:2165–2216. https://doi.org/10.1306/08121413151
Geertsma J, Haafkens R (1979) A comparison of the theories for predicting width and extent of vertical hydraulically induced fractures. J Energy Resour Technol 101:8–19. https://doi.org/10.1115/1.3446866
Gordeliy E, Peirce A (2013) Coupling schemes for modeling hydraulic fracture propagation using the XFEM. Comput Methods Appl Mech Eng 253:305–322. https://doi.org/10.1016/j.cma.2012.08.017
Gu H, Weng X, Lund JB et al (2012) Hydraulic fracture crossing natural fracture at nonorthogonal angles: a criterion and its validation. SPE Prod Oper 27:20–26. https://doi.org/10.2118/139984-PA
Guo X, Wu K, Killough J (2018) Investigation of production-induced stress changes for infill-well stimulation in Eagle Ford shale. SPE J 23:1–17. https://doi.org/10.2118/189974-PA
Gutenberg B, Richter CF (1942) Earthquake magnitude, intensity, energy, and acceleration. Bull Seismol Soc 32:163–191
Haddad M, Sepehrnoori K (2016) XFEM-based CZM for the simulation of 3D multiple-cluster hydraulic fracturing in quasi-brittle shale formations. Rock Mech Rock Eng 49:4731–4748. https://doi.org/10.1007/s00603-016-1057-2
Haddad M, Seperhrnoori K (2015) Simulation of hydraulic fracturing in quasi-brittle shale formations using characterized cohesive layer: stimulation controlling factors. J Unconv Oil Gas Resour 9:65–83. https://doi.org/10.1016/j.juogr.2014.10.001
Haddad M, Du J, Vidal-Gilbert S (2017) Integration of dynamic microseismic data with a true 3D modeling of hydraulic-fracture propagation in the Vaca Muerta shale. SPE J 22:1714–1738. https://doi.org/10.2118/179164-pa
Hou B, Zhang R, Zeng Y et al (2018) Analysis of hydraulic fracture initiation and propagation in deep shale formation with high horizontal stress difference. J Pet Sci Eng 170:231–243. https://doi.org/10.1016/j.petrol.2018.06.060
Howard G, Fast CR (1957) Optimum fluid characteristics for fracture extension. Proc Am Pet Inst 261–270
Hubbert MK, Willis DG (1957) Mechanics of hydraulic fracturing. Pet Trans AIME 210:153–168
Jackson RB, Vengosh A, Carey JW et al (2014) The environmental costs and benefits of fracking. In: Gadgil A, Liverman DM (eds) Annual review of environment and resources, annual reviews, vol 39. Palo Alto, California, pp 327–362

Jeffrey RG, Bunger A, LeCampion B, et al (2009) Measuring hydraulic fracture growth in naturally fractured rock. In: SPE Annual Technical Conference and Exhibition

Khristianovic SA, Zheltov YP (1955) Formation of vertical fractures by means of highly viscous liquid. 4th World Pet. Congr

King GE (2010) Thirty years of gas shale fracturing: what have we learned?. SPE Annu Tech Conf, Exhib

Kresse O, Weng X, Gu H, Wu R (2013) Numerical modeling of hydraulic fractures interaction in complex naturally fractured formations. Rock Mech Rock Eng 46:555–568. https://doi.org/10.1007/s00603-012-0359-2

Lecampion B (2009) An extended finite element method for hydraulic fracture problems. Commun Numer Methods Eng 25:121–133. https://doi.org/10.1002/cnm.1111

Lecampion B, Bunger A, Zhang X (2018) Numerical methods for hydraulic fracture propagation: a review of recent trends. J Nat Gas Sci Eng 49:66–83. https://doi.org/10.1016/j.jngse.2017.10.012

Lee B, Mack M, Maxwell S (2016) Completion optimization using a microseismically calibrated geomechanical hydraulic fracturing simulation in a naturally fractured formation. In: 50th US Rock Mechanics/Geomechanics Symposium

Li Q, Xing H, Liu J, Liu X (2015) A review on hydraulic fracturing of unconventional reservoir. Petroleum 1:8–15. https://doi.org/10.1016/j.petlm.2015.03.008

Lisjak A, Kaifosh P, He L et al (2017) A 2D, fully-coupled, hydro-mechanical, FDEM formulation for modelling fracturing processes in discontinuous, porous rock masses. Comput Geotech 81:1–18. https://doi.org/10.1016/j.compgeo.2016.07.009

Ma X, Zoback MD (2017) Lithology-controlled stress variations and pad-scale faults: a case study of hydraulic fracturing in the Woodford Shale, Oklahoma. Geophysics 82:ID35–ID44. https://doi.org/10.1190/geo2017-0044.1

Mack M, Zhang F, Lee BT et al (2016) Geomechanical modeling of microseismic depletion delineation. SEG Tech Progr Expand Abstr 2016:3006–3010

Mas Ivars D, Pierce ME, Darcel C et al (2011) The synthetic rock mass approach for jointed rock mass modelling. Int J Rock Mech Min Sci 48:219–244. https://doi.org/10.1016/j.ijrmms.2010.11.014

Maxwell S (2014) Microseismic imaging of hydraulic fracturing: improved engineering of unconventional shale reservoirs. Society of Exploration Geophysicists

Maxwell S, Cipolla C (2011) What does microseismicity tell us about hydraulic fracturing? SPE Annu Tech Conf Exhib

Maxwell S, Chorney D, Grob M (2015a) Differentiating wet and dry microseismic events induced during hydraulic fracturing. In: Unconventional Resources Technology Conference

Maxwell SC, Chorney D, Goodfellow SD (2015b) Microseismic geomechanics of hydraulic-fracture networks: insights into mechanisms of microseismic sources. Lead Edge 34:904–910. https://doi.org/10.1190/tle34080904.1

Maxwell SC, Zhang F, Damjanac B (2015c) Geomechanical modeling of induced seismicity resulting from hydraulic fracturing. Lead Edge 34:678–683. https://doi.org/10.1190/tle34060678.1

Maxwell SC, Lee BT, Mack M (2016) Calibrated microseismic geomechanical modeling of a Horn River basin hydraulic fracture. In: 50th US Rock Mechanics/Geomechanics Symposium

McGarr A (2014) Maximum magnitude earthquakes induced by fluid injection. J Geophys Res Earth 119:1008–1019. https://doi.org/10.1002/2013jb010597

Miehe C, Mauthe S (2016) Phase field modeling of fracture in multi-physics problems. Part III. Crack driving forces in hydro-poro-elasticity and hydraulic fracturing of fluid-saturated porous media. Comput Methods Appl Mech Eng 304:619–655. https://doi.org/10.1016/j.cma.2015.09.021

Mikelić A, Wheeler MF, Wick T (2015) Phase-field modeling of a fluid-driven fracture in a poroelastic medium. Comput Geosci 19:1171–1195. https://doi.org/10.1007/s10596-015-9532-5

Nagel NB, Sanchez-Nagel MA, Zhang F et al (2013) Coupled numerical evaluations of the geomechanical interactions between a hydraulic fracture stimulation and a natural fracture system in shale formations. Rock Mech Rock Eng 46:581–609. https://doi.org/10.1007/s00603-013-0391-x

Nordgren RP (1972) Propagation of a vertical hydraulic fracture. Soc Pet Eng J 12:306–314. https://doi.org/10.2118/3009-PA

Ouchi H, Katiyar A, Foster J, Sharma M (2015) A peridynamics model for the propagation of hydraulic fractures in heterogeneous, naturally fractured reservoirs. In: SPE Hydraulic Fracturing Technology Conference

Perkins TK, Kern LR (1961) Widths of hydraulic fractures. J Pet Technol. https://doi.org/10.2118/89-pa

Potyondy DO, Cundall PA (2004) A bonded-particle model for rock. Int J Rock Mech Min Sci 41:1329–1364. https://doi.org/10.1016/j.ijrmms.2004.09.011

Profit M, Dutko M, Yu J et al (2016) Complementary hydro-mechanical coupled finite/discrete element and microseismic modelling to predict hydraulic fracture propagation in tight shale reservoirs. Comput Part Mech 3:229–248. https://doi.org/10.1007/s40571-015-0081-4

Renshaw CE, Pollard DD (1995) An experimentally verified criterion for propagation across unbounded frictional interfaces in brittle, linear elastic materials. Int J Rock Mech Min Sci Geomech Abstr 32:237–249. https://doi.org/10.1016/0148-9062(94)00037-4

Roussel NP, Florez H, Rodriguez AA (2013) Hydraulic fracture propagation from infill horizontal wells. In: SPE Annual Technical Conference and Exhibition

Rubinstein JL, Ellsworth WL, Dougherty SL (2018) The 2013-2016 induced earthquakes in Harper and Sumner counties, southern Kansas. Bull Seismol Soc Am 108:674–689. https://doi.org/10.1785/0120170209

Safari R, Lewis R, Ma X et al (2017) Infill-well fracturing optimization in tightly spaced horizontal wells. SPE J 22:582–595. https://doi.org/10.2118/178513-PA

Siebrits E, Peirce AP (2002) A efficient multi-layer planar 3D fracture growth algorithm using a fixed mesh approach. Int J Numer Methods Eng 53:691–717. https://doi.org/10.1002/nme.308

Singh V, Roussel NP, Sharma MM (2008) Stress reorientation and fracture treatments in horizontal wells. SPE Annu Tech Conf Exhib

Snelling PE, de Groot M (2014) The effects of faults and fractures on microseismic in Horn River basin shales. In: CSEG GeoConvention 2014

Starfield AM, Cundall PA (1988) Towards a methodology for rock mechanics modelling. Int J Rock Mech Min Sci 25:99–106. https://doi.org/10.1016/0148-9062(88)92292-9

Tang J, Wu K (2018) A 3-D model for simulation of weak interface slippage for fracture height containment in shale reservoirs. Int J Solids Struct 144–145:248–264. https://doi.org/10.1016/j.ijsolstr.2018.05.007

Tang J, Wu K, Li Y et al (2018) Numerical investigation of the interactions between hydraulic fracture and bedding planes with non-orthogonal approach angle. Eng Fract Mech 200:1–16. https://doi.org/10.1016/j.engfracmech.2018.07.010

van der Elst NJ, Savage HM, Keranen KM, Abers GA (2013) Enhanced remote earthquake triggering at fluid-injection sites in the Midwestern United States. Science (80-) 341:164–167. https://doi.org/10.1126/science.1238948

Wang T, Zhou W, Chen J et al (2014) Simulation of hydraulic fracturing using particle flow method and application in a coal mine. Int J Coal Geol 121:1–13. https://doi.org/10.1016/j.coal.2013.10.012

Warpinski NR, Teufel LW (1987) Influence of geologic discontinuities on hydraulic fracture propagation. J Pet Technol. https://doi.org/10.2118/13224-pa

Warpinski NR, Mayerhofer M, Agarwal K, Du J (2013) Hydraulic-fracture geomechanics and microseismic-source mechanisms. SPE J. https://doi.org/10.2118/158935-pa

Weng X (2015) Modeling of complex hydraulic fractures in naturally fractured formation. J Unconv Oil Gas Resour 9:114–135. https://doi.org/10.1016/j.juogr.2014.07.001

Wileveau Y, Cornet FH, Desroches J, Blumling P (2007) Complete in situ stress determination in an argillite sedimentary formation. Phys Chem Earth 32:866–878. https://doi.org/10.1016/j.pce.2006.03.018

Wu K, Olson JE (2015) Simultaneous multifracture treatments: fully coupled fluid flow and fracture mechanics for horizontal wells. SPE J 20:337–342. https://doi.org/10.2118/167626-PA

Zhang F, Dontsov E (2018) Modeling hydraulic fracture propagation and proppant transport in a two-layer formation with stress drop. Eng Fract Mech 199:705–720. https://doi.org/10.1016/j.engfracmech.2018.07.008

Zhang F, Mack M (2016) Modeling of hydraulic fracture initiation from perforation Tunnels using the 3D lattice method. In: 50th US Rock Mechanics/Geomechanics Symposium 2016. American Rock Mechanics Association

Zhang F, Mack M (2017) Integrating fully coupled geomechanical modeling with microsesmicity for the analysis of refracturing treatment. J Nat Gas Sci Eng 46:16–25. https://doi.org/10.1016/j.jngse.2017.07.008

Zhang X, Jeffrey RG, Thiercelin M (2007) Deflection and propagation of fluid-driven fractures at frictional bedding interfaces: a numerical investigation. J Struct Geol 29:396–410. https://doi.org/10.1016/j.jsg.2006.09.013

Zhang F, Damjanac B, Huang H (2013a) Coupled discrete element modeling of fluid injection into dense granular media. J Geophys Res Solid Earth 118:1–20. https://doi.org/10.1002/jgrb.50204

Zhang F, Nagel N, Lee B, Sanchez-Nagel M (2013b) The influence of fracture network connectivity on hydraulic fracture effectiveness and microseismicity generation. In: 47th US Rock Mechanics/Geomechanics Symposium 2013

Zhang F, Maxwell S, Damjanac B (2015) Modeling of fault activation induced by hydraulic fracturing—a Horn River basin case study. Hydraul Fract J 2:26–33

Zhang F, Dontsov E, Mack M (2017) Fully coupled simulation of a hydraulic fracture interacting with natural fractures with a hybrid discrete-continuum method. Int J Numer Anal Methods Geomech 41:1430–1452. https://doi.org/10.1002/nag.2682

Zhang R, Hou B, Shan Q et al (2018) Hydraulic fracturing initiation and near-wellbore nonplanar propagation from horizontal perforated boreholes in tight formation. J Nat Gas Sci Eng 55:337–349. https://doi.org/10.1016/j.jngse.2018.05.021

Zhou J, Zhang L, Pan Z, Han Z (2016) Numerical investigation of fluid-driven near-borehole fracture propagation in laminated reservoir rock using PFC2D. J Nat Gas Sci Eng 36:719–733. https://doi.org/10.1016/j.jngse.2016.11.010

Zhu H, Shen J, Zhang F (2019) A fracture conductivity model for channel fracturing and its implementation with discrete element method. J Pet Sci Eng 172:149–161. https://doi.org/10.1016/j.petrol.2018.09.054